JOURNAL OF PETROLOGY | VOLUME 48 | NUMBER 6 | PAGES 1219–1241 | 2007 | doi:10.1093/petrology/egm015

Intermediate Alkali–Alumino-silicate Aqueous Solutions Released by Deeply Subducted Continental Crust: Fluid Evolution in UHP OH-rich Topaz–Kyanite Quartzites from Donghai (Sulu, China)

MARIA LUCE FREZZOTTI[1]*, SIMONA FERRANDO[2], LUIGI DALLAI[3] AND ROBERTO COMPAGNONI[2]

[1]DIPARTIMENTO DI SCIENZE DELLA TERRA, UNIVERSITÀ DEGLI STUDI DI SIENA, VIA LATERINA 8, I-53100 SIENA, ITALY

[2]DIPARTIMENTO DI SCIENZE MINERALOGICHE E PETROLOGICHE, UNIVERSITÀ DEGLI STUDI DI TORINO, VIA VALPERGA CALUSO 35, I-10125 TORINO, ITALY

[3]CNR–IGG, ISTITUTO DI GEOSCIENZE E GEORISORSE, VIA G. MORUZZI 1, I-56124 PISA, ITALY

RECEIVED APRIL 7, 2006; ACCEPTED MARCH 8, 2007
ADVANCE ACCESS PUBLICATION APRIL 17, 2007

Minerals, fluid inclusions and stable isotopes have been studied in ultrahigh-pressure (UHP) OH-rich topaz–kyanite quartzites from Hushan (west of Dongai), in southern Sulu (China). The quartzites underwent a metamorphic evolution characterized by a peak stage (3·5 GPa and 730–820°C) with the anhydrous assemblage coesite + kyanite I, followed by an early near-isothermal decompression stage (2·9 GPa and 705–780°C) with growth of kyanite II, muscovite, and OH-rich topaz, and by decompression-cooling stages, represented by paragonite (1·9 GPa and 700–780°C) and pyrophyllite (0·3 GPa and 400°C) on kyanite (I and II) and OH-rich topaz, respectively. These rocks may exhibit unusually low $\delta^{18}O$ and δD values acquired before undergoing UHP metamorphism. Five distinct fluid generations are recognized. Type I: concentrated peak solutions rich in Si, Al, and alkalis, present within multiphase inclusions in kyanite I. Type II: $CaCl_2$-rich brines present during the growth of early retrograde OH-rich topaz. Type III, IV, and V: late aqueous fluids of variable salinity, and rare CO_2 present during amphibolite- and late greenschist-facies conditions. A number of conclusions may be drawn from these relationships that have an effect on fluid evolution in deeply subducted continental rocks. (1) At a pressure of about 3·5 GPa alkali–alumino-silicate aqueous solutions, with compositions intermediate between H_2O fluid and melt ($H_2O > 25$ and ≤ 50 wt %) evolved from quartzites, probably generated by dehydration reactions. (2) During early decompression stages, at the transition from UHP to high-pressure (2·9 GPa) conditions, brines of external origin with higher water contents (82 wt % H_2O) initiated the growth of OH-rich topaz and muscovite. (3) The subsequent decompression, at $P < 2$ GPa, was defined by a limited circulation of NaCl aqueous fluids, and CO_2 infiltration. Overall, fluid inclusions and stable isotopes highlight a metamorphic fluid–rock interaction characterized by internally derived intermediate aqueous solutions at UHP, followed by infiltration of Cl-rich brines with higher water activities.

KEY WORDS: *ultrahigh-pressure metamorphism; OH-rich topaz; fluid inclusions; stable isotopes; supercritical liquids*

INTRODUCTION

Numerous discoveries of coesite and diamond in regional ultrahigh-pressure (UHP) rocks have demonstrated that crustal material can be subducted to mantle depths

*Corresponding author. Telephone: (+39) 0577 233929. Fax: (+39) 0577 233938. E-mail: frezzottiml@unisi.it

(Chopin, 1984; Smith, 1984; Sobolev & Shatsky, 1990), and provided new understanding of subduction and continental collision processes. The presence of aqueous fluids (± CO_2, N_2, etc.) at high-pressure (HP) and UHP conditions was recognized as the driving mechanism for metamorphic reactions, and ultimately for melting in crustal lithologies subducted to mantle depth (e.g. Poli & Schmidt, 2002). Our knowledge of fluid chemical properties is poor, yet is critical for understanding the potential concentration and transport of elements in the mantle wedge during subduction. One of the open questions concerns the nature and the amount of the chemical species in solution: moderate- to low-salinity aqueous fluids vs concentrated solutions, or hydrous melts.

One approach to obtaining information on the nature of fluids evolving from deep-subducted rocks is provided by fluid inclusion analysis combined with stable isotope geochemistry of natural UHP rocks, although the study of inclusions in these rocks is not an easy task. Peak metamorphic conditions are largely outside the isochore fields even for the densest fluids, and the exhumation P–T paths of the host rocks strongly favor decrepitation of the early trapped fluid inclusions (Touret, 2001). Despite these potential problems, a number of documented examples show that fluid inclusions can be preserved, providing valuable information on the composition of UHP fluids, and, to some extent, on their evolution (for reviews, see Scambelluri & Philippot, 2001; Touret & Frezzotti, 2003; Ferrando *et al.*, 2005*a*).

High-salinity aqueous fluid inclusions are often observed in UHP minerals. For example, in the UHP rocks from the Alps, fluid inclusions are characterized by high amounts of NaCl and $MgCl_2$, and subordinate concentrations of $CaCl_2$ and KCl (up to 50 wt % NaCl equiv.; Philippot & Selverstone, 1991; Selverstone *et al.*, 1992; Philippot *et al.*, 1995; Scambelluri *et al.*, 2001). To explain the NaCl-dominated nature of such HP solutions, Scambelluri *et al.* (1997) advocated recycled sea-water, Cl and alkalis, whereas Philippot *et al.* (1998) suggested that Cl-rich inclusions are derived from hydrothermal alteration of the oceanic lithosphere. More recently, Sharp & Barnes (2004) presented a model for the generation of brines, via breakdown of subducted serpentinites, forming mobile high-salinity aqueous plumes at mantle depths.

In the Dabie-Shan and Sulu UHP continental metamorphic rocks, fluids preserved within inclusions are also aqueous and salt-rich, but generally $CaCl_2$-dominated, and not NaCl-rich as would be expected if their ultimate origin was from past sea-water (Xiao *et al.*, 2000, 2001; Fu *et al.*, 2001, 2002, 2003; Zhang *et al.*, 2005b). Xiao *et al.* (2000) and Fu *et al.* (2001, 2003) described Ca-rich brines (±N_2), which may have originated during prograde and peak metamorphism. Zhang *et al.* (2005b) reported a spatial and temporal reconstruction of fluid composition within a vertical sequence of UHP rocks of different composition, and recognized primary $CaCl_2$–NaCl-rich brines as peak fluids in both eclogite and quartzite lithologies. As stable isotope data showed that brines are internally derived, Fu *et al.* (2003) proposed that they represent significant amounts of meteoric water brought to mantle depths through continental collision. Fluids reveal UHP metamorphism with limited fluid mobility during subduction, peak metamorphism, and exhumation.

Whereas previous studies indicated a substantial enrichment of chlorides in aqueous solutions at HP and UHP conditions, the presence in many UHP rocks of multiphase (or polyphase) solid inclusions, containing considerable amounts of hydrous alumino-silicate phases (e.g. amphiboles and micas), indicates transport of Si and Al (Ferrando *et al.*, 2005*a*, and references therein). These inclusions have been interpreted either as remnants of former UHP hydrous silicate melts, or as intermediate aqueous solutions (for a review, see Hermann *et al.*, 2006). As experimentally shown, the solubility of silica in aqueous fluids increases significantly at increasing pressure, as a result of complexing as polymers (Manning, 2004). Polymerization of silica enhances the transport of Ca, Na, K, and of those metal components (e.g. Al and Ti) that generally have low solubility in aqueous fluids (Antignano & Manning, 2005; Tropper & Manning, 2005). At extreme pressures, the amount of silica (±alumina) may reach high concentrations and give rise to intermediate silicate aqueous solutions. As pressure increases, the fluid–melt miscibility gap narrows, until the apex of the miscibility gap intersects the endpoint of the water-saturated solidus. Above this pressure, a single supercritical 'liquid' [in the sense of Kessel *et al.* (2005)] is present, with an intermediate composition between a hydrous silicate melt and a concentrated aqueous solution (e.g. 70–30 wt % H_2O), whose chemical and physical properties vary with temperature (Niggli, 1920; Stalder *et al.*, 2000).

The UHP rocks occurring in the Dabie–Sulu terranes in eastern China are of great interest to understanding the nature of fluids evolved from deeply subducted rocks. Here, continental lithologies have been carried down to a depth of at least 120–150 km and converted to eclogite-facies rocks, but have retained a number of original features, such as fluid inclusions in peak metamorphic minerals. These fluid inclusions represent samples of pristine fluids formed at UHP conditions, with a pre-metamorphic oxygen isotope signature that is heterogeneous at the outcrop scale and locally extremely ^{18}O-depleted (as low as $\delta^{18}O$ −10‰), caused by interaction with meteoric water prior to subduction (Yui *et al.*, 1995; Zheng *et al.*, 1996; Rumble & Yui, 1998; Rumble *et al.*, 2002).

The present study reports petrographic, fluid inclusion and stable isotope data for OH-rich topaz-bearing kyanite

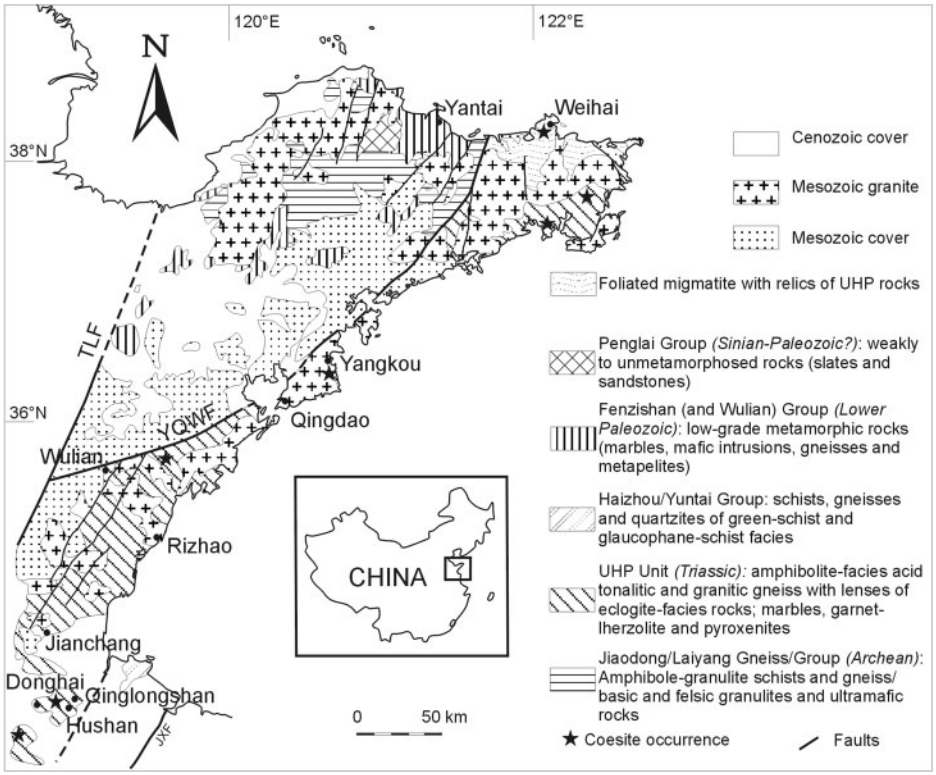

Fig. 1. Tectono-metamorphic sketch map of the Sulu terrane, eastern China, showing major tectonic units, occurrences of coesite and the location of Hushan, Donghai area. TLF, Tan-Lu fault; JXF, Jianshan–Xiangshui fault; YQWF, Yantai–Qingdao–Wulian fault.

quartzites from the Donghai area, southern Sulu terrane, and shows that internally derived aqueous fluids, with high concentrations of Si, Al, S, Ca, K and Na, but devoid of Cl, evolved at UHP conditions from continental rocks. During the early stages of decompression, the fluid composition changed into Ca-rich brines, probably of external origin. The present data allow us to model the chemical behavior of major elements in aqueous solutions generated at UHP conditions, and the overall fluid–rock interaction during the subsequent decompression stages, facilitating the reconstruction of the quartzite exhumation history.

REGIONAL GEOLOGY AND SAMPLE LOCATION

The Sulu terrane (Fig. 1) is the eastern end of the Qinling–Dabie orogen, which formed by the Triassic subduction and collision of the Yangtze craton beneath the Sino-Korean craton. Sulu is separated from Dabie Shan to the west by the Cretaceous left-lateral Tan-Lu fault (TLF) with a horizontal offset of about 500 km (Fig. 1). The Sulu terrane is bounded by the Yantai–Qingdao–Wulian fault (YQWF) to the NW and the Jianshan–Xiangshui fault (JXF) to the SE. It consists of a UHP, HP and migmatite metamorphic basement (Zhang *et al.*, 1995), intruded by post-orogenic Cretaceous granitic plutons. Mesozoic and more recent sediments constitute the youngest cover rocks (Wallis *et al.*, 1999). In the Sino-Korean craton, syn- and post-orogenic lamproites and lamprophyres are reported (Lu *et al.*, 1995; Guo *et al.*, 2004).

In the southern Sulu terrane, near Donghai (Fig. 1), the UHP unit consists of amphibolite-facies orthogneisses, ultramafic rocks, eclogites, amphibolites retrograded from eclogites, and paragneisses. Generally, eclogites occur in orthogneisses as layers and/or boudins wrapped by the main foliation of the host rocks. The eclogites are locally interlayered with paragneisses and quartzites (Zhang, R. Y., *et al.*, 1995; Zhang, Z., *et al.*, 2000). UHP eclogites from the Donghai area experienced a complex metamorphic history characterized by prograde, UHP peak, and retrograde metamorphism. The recent discovery of coesite in zircon from gneiss from Donghai and Taohang indicates that the country rocks also underwent regional UHP metamorphism (Ye *et al.*, 2000; Liu *et al.*, 2002). Prograde minerals (e.g. amphibole, paragonite, chlorite, staurolite, quartz, and phengite) may be preserved within peak garnet and pyroxene in eclogite (Wallis *et al.*, 1999, and references therein) and within the cores of zircons in paragneiss (Liu *et al.*, 2002).

Peak metamorphic conditions for eclogite are estimated at $T = 700$–$890^{\circ}C$ and $P > 2{\cdot}8$ GPa (Zhang *et al.*, 1995), and, more recently, at $T = 600$–$700^{\circ}C$ and $P = 3{\cdot}0$–$3{\cdot}5$ GPa (Mattinson *et al.*, 2004), at $T = 740$–$830^{\circ}C$ and $P = 3{\cdot}0$–$3{\cdot}9$ GPa (Zhang *et al.*, 2005*a*), and at $T = 790$–$890^{\circ}C$ and $P = 3{\cdot}5$–$4{\cdot}0$ GPa (Ferrando *et al.*, 2005b). Garnet and omphacite, occurring together with coesite as inclusions within zircon in paragneiss, also indicate peak conditions at $T = 815$–$850^{\circ}C$ and $P > 2{\cdot}8$ GPa (Liu *et al.*, 2001). The early stages of the retrograde P–T path are characterized by decompression with moderate cooling (from UHP/HP eclogite- to amphibolite-facies conditions), whereas late exhumation stages (from amphibolite- to greenschist-facies conditions) are dominated by cooling and moderate decompression (Zhang *et al.*, 1995; Ferrando *et al.*, 2005*b*).

In the Sulu eclogites, metamorphic Sm/Nd ages from 210 to 240 Ma have been obtained (Li *et al.*, 1993; Zhai *et al.*, 2000), which are consistent with U–Pb dating of zircons at 217 Ma (Ames *et al.*, 1996), and 228 Ma (Yang *et al.*, 2003). The protolith age of an eclogite from the Donghai area is constrained at 762 ± 28 Ma by whole-grain analysis of zircon (Ames *et al.*, 1996). Near Qinglongshan (Dongai area; Fig. 1), the rocks are characterized by oxygen and hydrogen isotope signatures acquired prior to subduction and preserved during subsequent prograde, UHP, and retrograde metamorphism. Extremely low $\delta^{18}O$ and δD values suggest that the protolith of these rocks interacted with fluids in a hydrothermal meteoric water system during a period of cold climate (Yui *et al.*, 1995; Zheng *et al.*, 1996, 1998; Rumble & Yui, 1998). Combined zircon U–Pb geochronology and oxygen isotope analysis of metagranites from this area indicates that the hydrothermal fluid–rock interaction took place in connection with late Proterozoic intrusions, possibly during the Sturtian glacial episode (Rumble *et al.*, 2002; Zheng *et al.*, 2003).

In the Donghai area, the quartz-rich rocks include a garnet–quartz–jadeite lithology, jadeite quartzite, garnet–quartz–phengite schist, phengite–quartz schist, and kyanite quartzite (Zhang, R. Y., *et al.*, 1995; Zhang, Z., *et al.*, 2000). Among the kyanite quartzites, two types were identified by Zhang *et al.* (1996): Type 1: coesite pseudomorph-bearing quartzites interlayered with eclogites, and consisting of quartz, epidote, kyanite, and minor omphacite, garnet, phengite, and rutile; Type 2: kyanite quartzites, consisting of quartz, kyanite (including rutile and polycrystalline quartz aggregates after coesite), and accessory pyrite. In the latter, OH-rich topaz has been reported at Fushan, west of Dongai (Zhang *et al.*, 2002). Five specimens of Type 2 kyanite quartzite from Hushan (west of Donghai; Fig. 1), which in all probability corresponds to the locality named Fushan by Zhang *et al.* (2002), were sampled from trenches 3 m deep to the SW of a ridge consisting of orthogneiss.

ANALYTICAL METHODS

The chemical compositions of minerals were determined using both a JEOL-JXA 8600 electron microprobe, using wavelength dispersive spectrometry (WDS), at the CNR–IGG in Firenze, and a Cambridge Instruments Stereoscan 360 scanning electron microscope equipped with an energy-dispersive spectrometry (EDS) system at the Dipartimento di Scienze Mineralogiche e Petrologiche in Torino. WDS analyses were performed using 15 kV accelerating voltage, 20 nA beam current, 100 s counting time for each point analysis, and a beam diameter of 5 μm. Standards were: albite (Si, Na), ilmenite (Ti, Fe), plagioclase (Al), chromite (Cr), rhodonite (Mn), olivine (Mg), diopside (Ca), sanidine (K), fluorite (F), tugtupite (Cl). Operating conditions for EDS analyses were 15 kV accelerating voltage, 1·35 nA beam current, and 50 s counting time. Natural minerals and pure oxides were used as standards. The chemical composition of OH-rich topaz was calculated as described by Alberico *et al.* (2003). Structural formulae of minerals were processed using the program by Ulmer (1986). Mineral abbreviations are after Kretz (1983).

Microthermometry of fluid inclusions was performed on doubly polished, 100–150 μm thick, sections using a Linkam THMSG600 heating–freezing stage coupled with a microscope equipped with 40× or 100× objectives, at the Universities of Siena and Torino.

The stages were calibrated by a set of synthetic fluid inclusions with an estimated accuracy of about $\pm 0{\cdot}1^{\circ}C$ at the triple point of CO_2 ($-56{\cdot}6^{\circ}C$), at the triple point of H_2O ($0{\cdot}015^{\circ}C$), and at the critical temperature of H_2O ($374^{\circ}C$). Freezing temperature (T_f), eutectic temperature (T_e), final melting temperature (T_m), and homogenization temperature (T_h) were measured during heating–freezing cycles. Heating rates were $0{\cdot}1^{\circ}C$/min approaching T_m, and $0{\cdot}5^{\circ}C$/min approaching T_h. Microthermometric data to obtain fluid inclusion compositions, densities, and isochores were processed with the software packages FLUID 1 (Bakker, 2003).

Laser Raman analyses were made with a Labram microspectrometer (Horiba, Jobin Yvon Ltd) at the University of Siena. The excitation source was a polarized Ar^{+}-ion laser operating at 514·5 nm wavelength, and 200–550 mW incident power. The laser spot size was focused to 1–2 μm with a 100× objective. Accumulation times were in the range 20–90 s. The 1332 cm^{-1} diamond band was used for the daily calibration.

Oxygen isotope compositions of mineral separates were measured at the CNR–IGG of Pisa, using the laser fluorination technique of Sharp (1990). Mineral separates were obtained from crushed, sieved (0·3 and 0·5 mm fraction), and ultrasonically cleaned samples. Pure mineral fractions (>99 vol. %) of quartz, kyanite, topaz and rutile were obtained by means of standard heavy liquid techniques, followed by hand-picking under a binocular microscope.

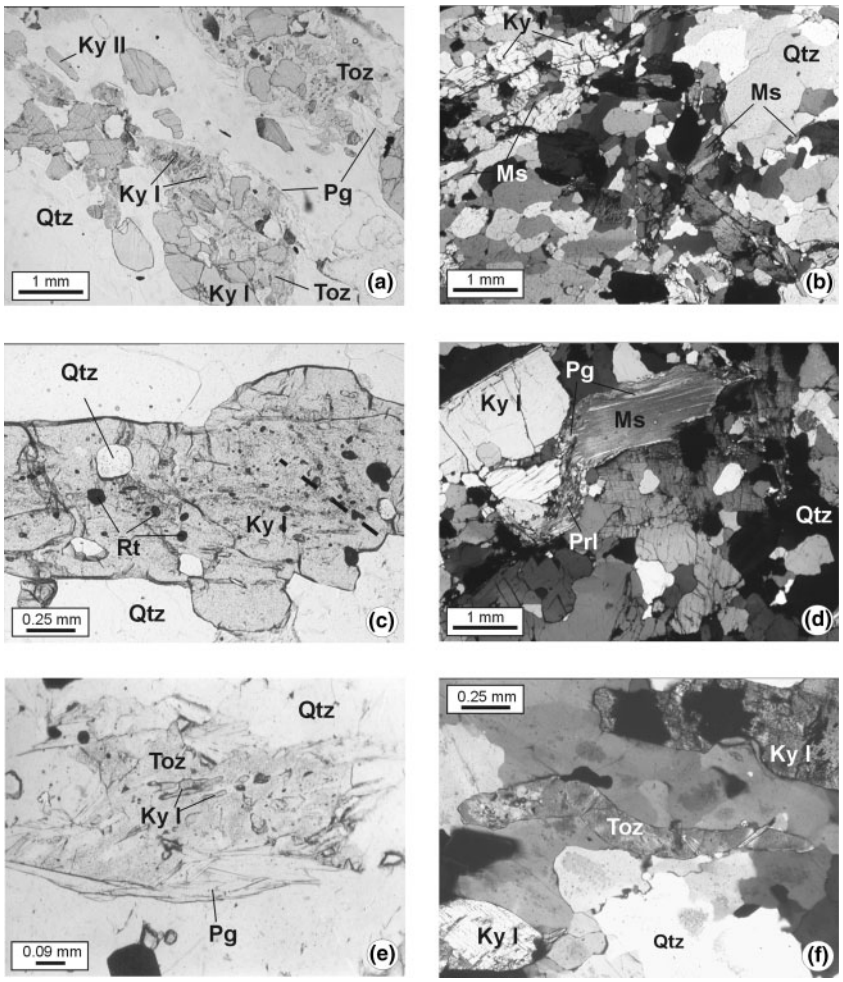

Fig. 2. Photomicrographs illustrating mineral associations in the quartzites from Hushan. (a) Weakly foliated quartzite, consisting of quartz, kyanite, OH-rich topaz, and paragonite. Two generations of kyanite may be recognized: porphyroclastic Ky I, sometimes preserved as relics within OH-rich topaz, and a fine-grained Ky II, which defines the rock foliation. A retrograde paragonite corona is rimming OH-rich topaz. Sample RPC 78l; plane-polarized light (PPL). (b) Growth of muscovite after Ky I. Sample RPC 544; crossed polars (CP). (c) Ky I porphyroclast including polycrystalline quartz after coesite, and rutile. Very fine-grained zircon crystals define an isoclinally folded S_i; the dashed line shows the axial plane of a fold. Sample RPC 782; PPL. (d) Muscovite flake mantled and partly replaced by paragonite. Aggregates of pyrophyllite grow at the contact with kyanite. Sample RPC 545; CP. (e) OH-rich topaz crystal including relict Ky I, rimmed by retrograde paragonite. Sample RPC 547; PPL. (f) Undeformed OH-rich topaz crystal developed at the expense of a deformed Ky II. Sample RPC 78l; CP. Mineral abbreviations are after Kretz (1983).

Analyses on about 1–1·5 mg of material were duplicated and averaged. A 15 W Merchantek CO_2 laser was used for heating the sample in a F_2 atmosphere. The $\delta^{18}O$ values were measured on a Finnigan MAT Delta Plus mass spectrometer. The analytical precision was monitored by using the laboratory standards QMS and Lausannel ($\delta^{18}O$ values were 14·05 and 18·1‰, respectively), and was always better than 0·12‰ (1σ). During this study the average composition of NBS 28 at CNR–IGG was $9{\cdot}54 \pm 0{\cdot}17$‰ ($n = 9$). All isotope values are reported in the conventional $\delta^{18}O$ notation relative to SMOW. The D/H ratios of paragonite and topaz were also measured at the CNR–IGG, and duplicated at the University of Budapest for intercomparison by conventional vacuum fusion, following the method of Vennemann & O'Neil (1993). The δD values were compared with those of an internal standard, calibrated relative to NBS-30 ($\delta D = -67$‰).

PETROGRAPHY AND MINERAL CHEMISTRY

The studied quartzites are weakly foliated, medium- to coarse-grained, and consist of quartz (or coesite) (~70–80 vol. %), kyanite (~10–20 vol. %), white mica (up to 5 vol. %) ±OH-rich topaz, ±pyrophyllite, and

Table 1: Representative chemical analyses of kyanite and OH-rich topaz from Hushan quartzite

	EDS	EDS	EDS	EDS	EDS	EDS	EDS	EDS	EDS	EDS	EDS	WDS
Sample:	RPC542	RPC542	RPC542	RPC542	RPC542	RPC544	RPC544	RPC544	RPC545	RPC546	RPC547	RPC 547
Mineral:	Ky	Ky	Ky	Ky	Ky	Ky	Ky	Ky	Ky	Ky	Ky	Toz*
Analysis:	IIIKy12	IIIKy13	IIIKy14	IIIKy22	4Ky25	VKy50	VKy52	VKy54	12Ky1	6Ky11	IIKy66	
SiO_2	37·3	37·3	37·2	36·9	36·7	37·0	37·1	37·0	37·5	37·7	37·0	33·58 (0·20)
Al_2O_3	62·7	61·7	62·3	61·8	62·0	61·4	61·9	62·1	63·4	63·2	62·1	56·97 (0·22)
Fe_2O_3†	0·6	0·0	0·8	1·2	1·1	0·3	0·5	0·5				0
FeO	0·1	0·5	0·1	0·0	0·0	0·4	0·3	0·1	<0·1	<0·1	<0·1	0·02 (0·02)
F												15·35 (0·57)
Cl												<0·03
H_2O†												2·77 (0·30)
Total	100·7	99·5	100·5	99·9	99·7	99·1	99·7	99·8	100·9	100·9	99·1	108·69 (0·14)
F,Cl = O												6·46 (0·24)
Total												99·46 (0·08)
Si	1·00	1·01	1·00	1·00	1·00	1·01	1·01	1·00	1·00	1·01	1·01	1·00
Al	1·98	1·98	1·98	1·98	1·98	1·98	1·98	1·98	2·00	1·99	1·99	2·00
Fe^{3+}	0·01	0·00	0·02	0·02	0·02	0·01	0·01	0·01				0·00
Fe^{2+}	0·00	0·01	0·00	0·00	0·00	0·01	0·01	0·00				0·00
F												1·45
OH												0·55
X_{OH}												0·28

*Average of 15 WDS analyses of OH-rich topaz. Standard deviations are given in parentheses. From Alberico *et al.* (2003).
†Fe_2O_3 and H_2O calculated using the program by Ulmer (1986).

accessory rutile, pyrite, zircon, apatite, ±barite and diaspore (Fig. 2a and b). Two kyanite generations are present: an early coarse-grained kyanite (Ky I), which occurs as stubby crystals with no preferred orientation, and a later medium-grained prismatic kyanite (Ky II), whose preferred orientation defines a weak foliation (Fig. 2a). Kyanite I includes polycrystalline quartz (after coesite), rutile, zircon, and fluid inclusions, and rarely preserves a folded S_i defined by alignment of very fine-grained quartz or zircon crystals (Fig. 2c). Kyanite II is locally deformed and has no inclusions of polycrystalline quartz, single quartz crystals, or fluids. In some samples, both kyanite generations show a weak bluish color, as a result of the presence of minor amounts of iron [Fe_{tot} ≤0·02 atoms per formula unit (a.p.f.u.); Table 1].

White mica consists of both muscovite and paragonite, in variable amounts. Muscovite occurs as medium- to fine-grained flakes typically grown on Ky I, and rarely on Ky II (Fig. 2b). Silicon ranges from 3·04 to 3·17 a.p.f.u., Na is up to 0·37 a.p.f.u., and Mg does not exceed 0·09 a.p.f.u. (Table 2). Muscovite shows high F contents for metamorphic rocks [up to 0·44 wt %: $X_{OH} = OH/(OH + F) = 0·95–0·96$], but no Cl. Late paragonite is also present, and occurs as randomly oriented flakes forming more or less continuous coronae that mantle kyanite I and II, topaz, and locally muscovite (Fig. 2a, d and e). Minor paragonite is additionally found as fine-grained crystals within mineral fractures. The Na content ranges from 0·72 to 0·94 a.p.f.u., and the K content is <0·22 a.p.f.u.; Table 2). Fluorine ranges from 0·48 to 0·89 wt % ($X_{OH} = 0·91–0·95$). In the most retrogressed samples, minor amounts of pyrophyllite containing F (≤0·30 wt %; X_{OH} ≤0·98; Table 2) developed at the expense of kyanite, locally overgrowing paragonite (Fig. 2d).

OH-rich topaz occurs sporadically in some horizons, where it may constitute up to 10 vol. %. The OH-rich topaz is clearly retrograde and developed at the expense of both Ky I and Ky II. In topaz, Ky I relics are often observed as corroded and oriented fine-grained crystals showing uniform extinction (Fig. 2a), whereas topaz completely replaces Ky II. Although a few OH-rich topaz grains appear to be deformed, they always show homogeneous extinction (Fig. 2f), indicating pseudomorphous replacement after former deformed Ky II, oriented along the main foliation. OH-rich topaz includes rutile and

Table 2: Representative EDS analyses of muscovite, paragonite, and pyrophyllite from the Hushan quartzite

	EDS	EDS	EDS	EDS	EDS	EDS	EDS	EDS	EDS	EDS	WDS	WDS
Sample:	RPC542	RPC542	RPC542	RPC542	RPC542	RPC542	RPC545	RPC545	RPC545	RPC545	RPC 545	RPC 545
Analysis:	IIIMs15	IIIMs16	IIIMs17	IIIMs21	IVMs23	IVMs24	12Ms9	12Ms11	12Ms22	12Ms49	15Wm11	12Wm21
SiO_2	47·2	47·2	47·3	45·8	46·1	46·6	46·6	46·5	47·1	46·5	45·56	45·90
TiO_2	0·5	<0·1	<0·1	0·6	0·5	0·6	0·6	0·6	0·5	0·4	0·36	0·26
Al_2O_3	34·8	33·9	34·6	36·0	35·3	34·6	36·8	36·1	36·6	36·7	36·12	36·35
Fe_2O_3*	0·0	0·0	0·0	0·0	0·0	0·0	0·0	0·5	0·5	0·0	0·92	1·20
FeO	1·0	1·1	1·0	1·1	1·1	1·0	0·9	0·4	0·4	0·9	0·00	0·00
MgO	0·7	0·9	0·8	0·3	0·5	0·5	<0·2	0·5	0·6	<0·2	0·43	0·49
Na_2O	1·4	1·1	1·4	1·6	1·3	1·1	2·9	2·3	2·7	2·6	1·25	2·32
K_2O	9·7	10·3	9·7	9·7	10·1	10·3	7·5	8·1	7·9	7·5	10·51	7·88
F	<0·3	<0·3	<0·3	<0·3	<0·3	<0·3	<0·3	<0·3	<0·3	<0·3	0·39	0·44
Cl	<0·2	<0·2	<0·2	<0·2	<0·2	<0·2	<0·2	<0·2	<0·2	<0·2	<0·03	<0·03
H_2O*	4·5	4·5	4·5	4·5	4·5	4·5	4·6	4·5	4·6	4·5	4·30	4·32
Total	99·9	99·0	99·3	99·6	99·4	99·1	99·9	99·4	100·8	99·3	99·84	99·21
F,Cl = O											0·16	0·19
Total											99·68	99·02
Si	3·13	3·17	3·15	3·05	3·08	3·13	3·07	3·07	3·06	3·07	3·05	3·04
Ti	0·02			0·03	0·03	0·03	0·03	0·03	0·03	0·02	0·02	0·01
Al	2·72	2·68	2·72	2·83	2·78	2·74	2·85	2·81	2·81	2·86	2·85	2·84
Fe^{3+}	0·00	0·00	0·00	0·00	0·00	0·00	0·00	0·02	0·02	0·00	0·07	0·06
Fe^{2+}	0·06	0·06	0·06	0·06	0·06	0·05	0·05	0·02	0·02	0·05	0·00	0·00
Mg	0·07	0·09	0·08	0·03	0·05	0·05		0·05	0·06		0·04	0·05
Na	0·18	0·15	0·18	0·20	0·16	0·14	0·37	0·30	0·33	0·34	0·16	0·30
K	0·82	0·88	0·82	0·83	0·86	0·88	0·63	0·68	0·65	0·64	0·90	0·67
F											0·08	0·09
OH	2·00	2·00	2·00	2·00	2·00	2·00	2·00	2·00	2·00	2·00	1·92	1·91
X_{OH}											0·96	0·95

	EDS	EDS	EDS	EDS	EDS	EDS	WDS	WDS	WDS	WDS	WDS	WDS
Sample:	RPC545	RPC545	RPC545	RPC546	RPC546	RPC546	RPC546	RPC546	RPC546	RPC546	RPC545	RPC545
Analysis:	12Pg23	12Pg30	12Pg32	1Pg3	7Pg27	7Pg30	1Pg1	2Pg2	2Pg3	3Pg20	12Prl23	12Prl24
SiO_2	47·8	47·8	47·7	47·1	47·8	47·4	47·44	47·03	46·94	47·51	65·26	65·53
TiO_2	<0·1	<0·1	<0·1	<0·1	<0·1	<0·1	0·06	0·10	0·04	0·04	0·07	<0·03
Al_2O_3	38·9	39·1	39·1	39·4	39·4	39·1	40·00	39·64	39·13	39·36	28·33	28·03
Fe_2O_3*	0·7	0·5	0·2	0·6	0·0	0·0	0·30	0·33	0·27	0·38	0·36	0·20
FeO	0·0	0·0	0·3	0·0	0·0	<0·1	0·00	0·00	0·00	0·00	0·00	0·00
MgO	<0·2	<0·2	<0·2	<0·2	<0·2	<0·2	<0·06	<0·06	<0·06	<0·06	0·10	<0·06
Na_2O	6·0	5·9	6·2	7·3	7·2	7·2	7·15	7·40	7·17	7·64	0·05	0·28
K_2O	2·6	2·8	2·6	0·4	0·7	0·4	0·27	0·48	0·59	0·31	0·02	0·09
F	<0·3	<0·3	<0·3	<0·3	<0·3	<0·3	0·67	0·55	0·48	0·89	0·30	0·21
Cl	<0·2	<0·2	<0·2	<0·2	<0·2	<0·2	<0·03	<0·03	<0·03	<0·03	<0·03	<0·03
H_2O*	4·7	4·7	4·7	4·7	4·7	4·7	4·42	4·45	4·43	4·29	4·81	4·87
Total	100·7	100·8	100·7	99·5	99·8	99·3	100·31	99·98	99·05	100·42	99·30	99·21
F,Cl = O							0·28	0·23	0·21	0·37	0·13	0·09
Total							100·03	99·75	98·84	100·05	99·17	99·12
Si	3·04	3·04	3·04	3·01	3·04	3·03	3·00	3·00	3·02	3·02	7·89	7·91
Ti							0·00	0·00	0·00	0·00	0·01	—

(continued)

Table 2: Continued

	EDS	EDS	EDS	EDS	EDS	EDS	WDS	WDS	WDS	WDS	WDS	WDS
Sample:	RPC545	RPC545	RPC545	RPC546	RPC546	RPC546	RPC546	RPC546	RPC546	RPC546	RPC545	RPC545
Analysis:	12Pg23	12Pg30	12Pg32	1Pg3	7Pg27	7Pg30	1Pg1	2Pg2	2Pg3	3Pg20	12Prl23	12Prl24
Al	2·92	2·93	2·93	2·96	2·96	2·95	2·98	2·98	2·96	2·95	4·04	3·99
Fe^{3+}	0·03	0·02	0·01	0·03	0·00	0·03	0·01	0·02	0·01	0·02	0·03	0·02
Fe^{2+}	0·00	0·00	0·02	0·00	0·00	0·00	0·00	0·00	0·00	0·00	0·00	0·00
Mg											0·02	
Na	0·74	0·72	0·77	0·90	0·89	0·89	0·88	0·91	0·89	0·94	0·01	0·07
K	0·21	0·22	0·21	0·03	0·06	0·03	0·02	0·04	0·05	0·03	0·00	0·01
F							0·13	0·11	0·10	0·18	0·11	0·08
OH	2·00	2·00	2·00	2·00	2·00	2·00	1·87	1·89	1·90	1·82	3·88	3·92
X_{OH}							0·93	0·94	0·95	0·91	0·97	0·98

*Fe_2O_3 and H_2O calculated using the program by Ulmer (1986).

zircon, but no quartz. Rare diaspore, formed after relic kyanite, is locally present. Topaz is rich in fluid inclusions, which may be locally so abundant as to make it 'dusty' under the optical microscope. The significant amounts of OH-bonds in the topaz structure are revealed by Raman spectroscopic analyses with an intense vibration at 3637 cm^{-1} (not shown). WDS and X-ray diffraction analyses indicate a mean OH content with $X_{OH} = OH/(OH + F) = 0{\cdot}28$ (Table 1; Alberico *et al.*, 2003) without any evident zoning from the core to the rim. Such X_{OH} value is in the range for topaz crystals from Fushan (X_{OH} from 0·28 to 0·39) reported by Zhang *et al.* (2002).

FLUID INCLUSIONS

Petrography, microthermometry, and Raman microspectroscopy

Aqueous fluid inclusions in quartzite are generally solute-rich with different solutes. Carbonic fluids are rare. Inclusion distribution is limited and localized within single minerals: primary inclusions are observed both in peak Ky I, and in OH-rich topaz, whereas late intra- and inter-granular inclusion trails occur in matrix quartz. Kyanite II and quartz after coesite do not contain fluid inclusions. Five fluid inclusion populations are discussed in the following sections, according to their relative timing of trapping. A selection of representative analytical results is reported in Table 3.

Primary alumino-silicate-rich multiphase solid inclusions in kyanite I (Type I)

Within porphyroclastic Ky I, multiphase solid inclusions are distributed randomly, or along short planes of original healed microfractures (Fig. 3a). These inclusions typically contain a variety of mineral phases, one or more deformed bubbles, but no liquid phase (Fig. 3b). Such inclusions, which are found also in peak phases of UHP eclogite from the same locality, have been the subject of a previous detailed petrographic study, which aimed at reconstructing their original chemical composition (Ferrando *et al.*, 2005*a*). Here, we summarize the major characteristics. Paragonite, muscovite, and anhydrite constitute the dominant mineral assemblage within the inclusions, with rather constant volume proportions, indicating that these are daughter minerals (Fig. 3b). A second sulfate phase containing Al and variable amounts of K and Na is often observed, which has been identified by Raman spectroscopy as an hydroxyl-bearing K–Na-sulfate [possibly alunite-type: $KAl_3(SO_4)_2(OH)_6$; Ferrando *et al.*, 2005*a*]. Chlorides (e.g. halite) are absent. Additional phases may include corundum and diaspore, calcite, chlorite, barite, pyrite, and apatite, which are considered incidentally trapped phases [see Ferrando *et al.* (2005*a*) for a discussion of secondary processes]. A semi-quantitative estimate of volumetric proportions indicates that Type I inclusions contain approximately 20% paragonite, 20% 'alunite-type' sulfate, 20% muscovite, 15% anhydrite, and 20–30% of 'fluid'. The remaining 5 vol. % consists of one or more incidentally trapped phases.

Primary Ca-rich brine inclusions in OH-rich topaz (Type II)

In OH-rich topaz, fluid inclusions are extremely abundant in the central portions of the crystals, whereas they are systematically absent from the rims (Fig. 3c; primary fluid inclusions, Roedder, 1984). They are generally two- or three-phase aqueo-carbonic (L_{CO2}–L_{H2O}, and V_{CO2}–L_{CO2}–L_{H2O}) and show rounded or negative crystal

Table 3: Representative microthermometric data for fluid inclusions from Hushan quartzite

Sample	Host mineral	f.i. type	T_{fCO2} (°C)	T_{mCO2} (°C)	T_{hCO2} (°C)	T_{fH2O} (°C)	T_e (°C)	T_{mHhl} (°C)	T_{mice} (°C)	T_{hH2O} (°C)
546-1 A	Toz	II	−96·0	−56·6	9·4	−57·5	−46·9	−32·0	−11·8	
546-1 A	Toz	II	95·5	−56·6	8·7	59·9	46·0		−13·0	
546-1 A	Toz	II	95·0	−56·6	9·7			−35·0		
546-1 A	Toz	II	−96·8		14·9				−19·0	
546-1 A	Toz	II	−96·0	−56·8	20·2	−58·0	−42·0		−10·0	
546-1 B	Toz	II	−96·5	−56·6	21·6					
546-1 A	Toz	II	−93·0	−56·5	28·6	−69·7	−52·3			
546-1 A	Toz	II	−95·4	−56·7	28·6					
546-1 A	Toz	II	−94·3	−56·7	29·7	−60·0	−54·0		−12·8	
546-1 A	Toz	II			−7·7					
546-1 A	Toz	II	−95·4	−56·6	30·9	−64·6	−46·0			
546-1 A	Toz	II	−96·0	−56·6	**31·0**			−30·0		
546-1 A	Toz	II	−94·8	−56·7	*30·9*	−61·2		−33·4	12·0	
547/14b B	Toz	II	−96·9	−56·5	−1·6				−14·0	
547/14b B	Toz	II	−95·0	−56·6	12·1	−65·0	−50·5			
547-14bA	Toz	II	−96·8	−56·6	13·3			−25·3		
547-2	Toz	II			*31·0*					
547-1	Toz	II	−96·2	−56·5	**27·5**	−69·5	−45·0	−25·3		
546-1a	Toz	II	−96·0	−56·5	30·4				−7·1	
547-12dA	Qtz	III				−38·5	−30·6	−22·2	−7·3	231·7
547-12dA	Qtz	III				−37·2	−28·9	−19·0		177·1
547-12dA	Qtz	III					−31·2	−22·4	−7·6	204·9
547-12dA	Qtz	III				−36·6	−28·1	−19·8	−7·5	215·2
547-12dA	Qtz	III					−34·4	−24·8	−6·6	259·5
547-12dB	Qtz	III				−36·5			4·8	233·9
547-17A	Qtz	III				−35·0	−33·3		−6·4	198·1
547-17A	Qtz	III				−37·8	34·8		−6·9	170·7
547-17A	Qtz	III							−5·4	101·5
547-17A	Qtz	III							−4·8	134·9
544-13bG	Qtz	IV	−95·3	−56·8/−56·7	6·4					
544-13bG	Qtz	IV	−95·2	−56·8/−56·7	7·2					
544-13bG	Qtz	IV	−95·5	−56·8/−56·7	7·8					
544-13bG	Qtz	IV	−96·0	−56·8/−56·7	−4·4					
544-13bG	Qtz	IV	−95·3	−56·6	9·5					
544-13bG	Qtz	IV	−95·4	−56·6	5·4					
544-13bG	Qtz	IV	−95·5	−56·6	7·2					
547/14b B	Qtz	IV	−95·5	−56·8/−56·7	7·8					
547/14b B	Qtz	IV	−95·3	−56·6	7·0					
547/14b B	Qtz	IV	−94·7	−56·6	7·1					
547-14bD	Qtz	V				−36·6	−23·7		−5·7	209·5
547-14bD	Qtz	V				−36	−21·7		−6·5	211·4
547-14bD	Qtz	V				−32·1			−6·5	
547-14bD	Qtz	V				−36	−20·7		−6·2	206·5
547-14bD	Qtz	V							−5·2	102·3
547-17A	Qtz	V								222·3
547-17A	Qtz	V				−33·3	−21·3		−4·7	121·3

f.i., Fluid inclusion; T_f, temperature of freezing; T_e, eutectic temperature; T_m, temperature of melting; T_h, temperature of homogenization; Hhl, hydrohalite. Homogenization temperatures are to the liquid phase, with the exception of those shown in bold type, which are to the vapor phase, and those in italics, which are critical.

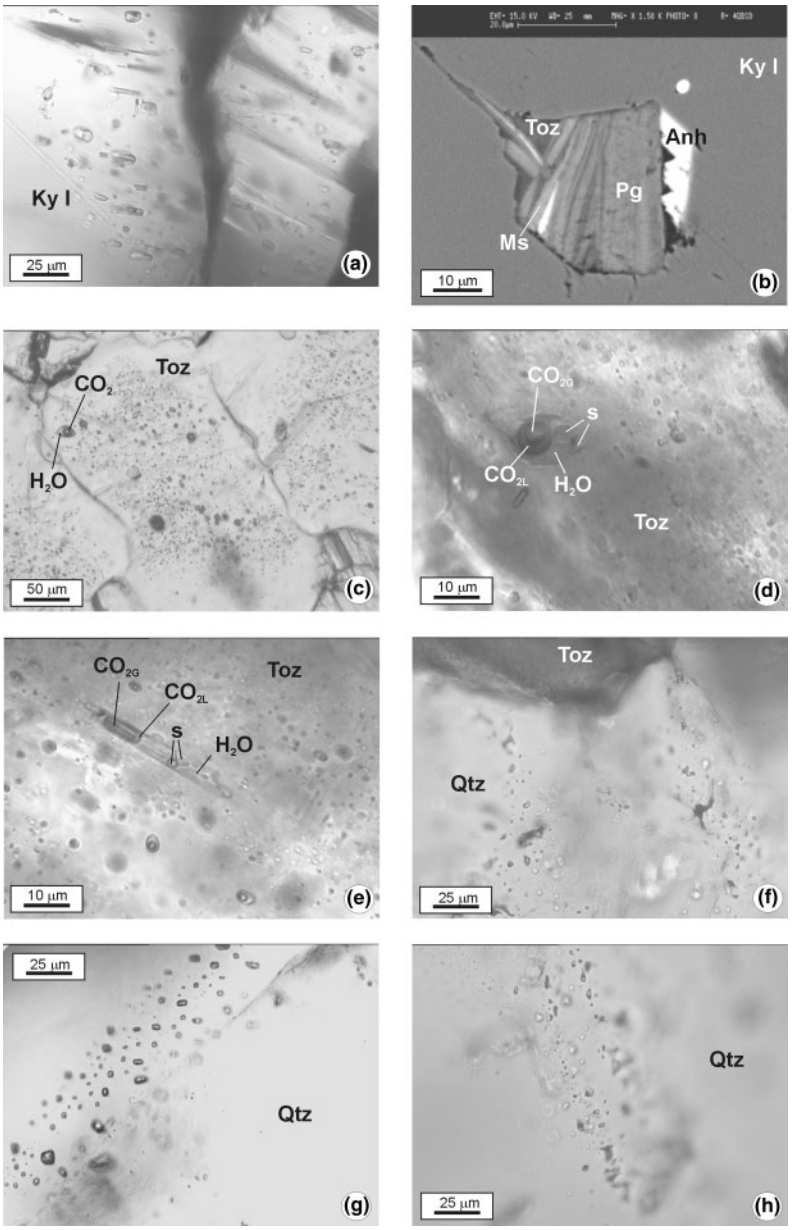

Fig. 3. Photomicrographs illustrating the different types of inclusions present within the quartzites from Hushan. (a) Distribution of Type I multiphase solid inclusions within Ky I. Sample RPC 542; PPL. (b) Back-scattered electron image of a decrepitated multiphase solid inclusion in Ky I, showing the typical association of paragonite + muscovite + anhydrite + cavities (in black). Sample RPC 547. (c) Distribution of Type II primary fluid inclusions in OH-rich topaz. Sample RPC 546; PPL. (d) Large rounded Type II brine inclusion containing liquid and gaseous CO_2 (about 30% of the inclusion total volume), and two solids (s). Sample RPC 546; PPL. (e) Type II fluid inclusion elongated parallel to the *c*-axis of the host OH-rich topaz. The composition of the inclusion is similar to that described in (d). Sample RPC 547; PPL. (f) Type III aqueous fluid inclusions in quartz. The fluid inclusions occur as short intragranular trails, originating from the OH-rich topaz. Sample RPC 547; PPL. (g) Type IV CO_2 ($\pm$ N_2) fluid inclusions in quartz. The fluid inclusions occur as intragranular trails. Site RPC 544/13bG; PPL. (h) Trail of Type V aqueous fluid inclusions in quartz. Sample RPC 547/14bD; PPL.

shapes (5–50 μm in size). Only some fluid inclusions contain daughter crystals, defining a four-phase assemblage (V_{CO2}–L_{CO2}–L_{H2O}–S). The most common daughter phase is halite, followed by gypsum and anhydrite (Fig. 3d and e), both identified by Raman microspectroscopy (Fig. 4). Within each inclusion, CO_2 varies from 5 to 50% of the total volume. There is an observed correlation between size of the inclusions, CO_2, and daughter mineral content: larger inclusions generally contain daughter minerals and a larger volume per cent of low-density CO_2 (i.e. two-phase, L + V) than smaller ones (Fig. 3d and e).

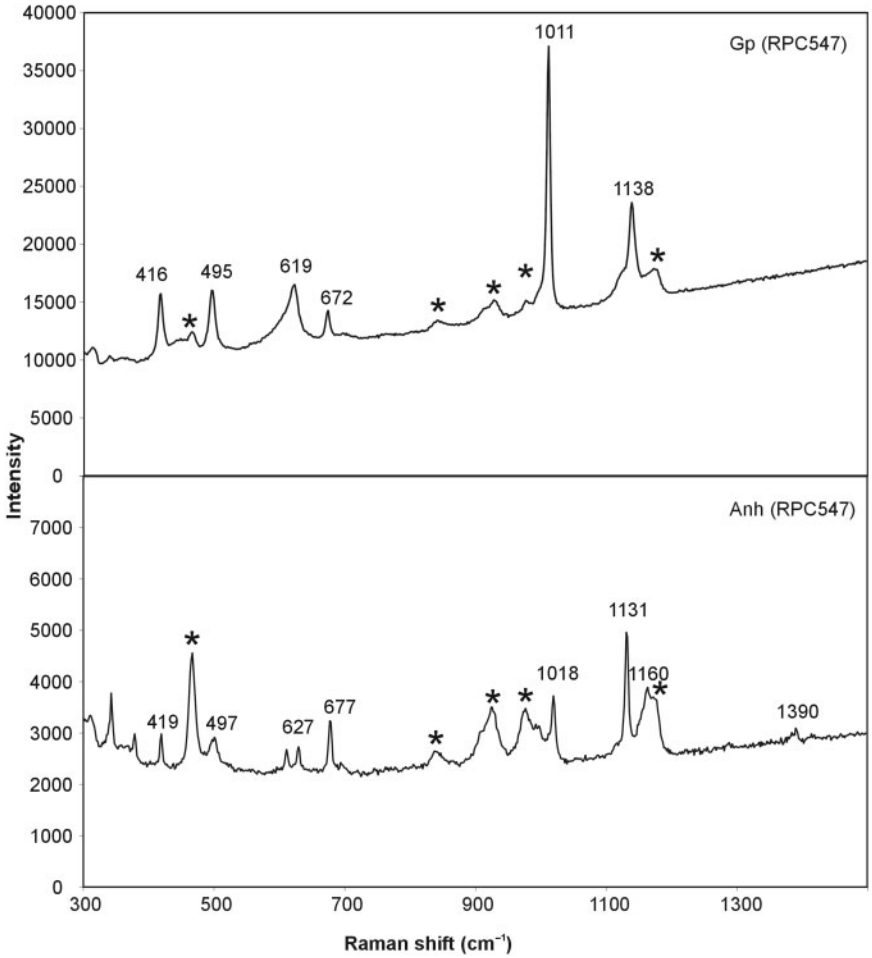

Fig. 4. Representative Raman spectra for daughter sulfates within Type II fluid inclusions: gypsum (Gp; top) and anhydrite (Anh; bottom). The peaks at 1011 and 1118 cm^{-1} are characteristic for sulfates. The peaks with asterisks represent the host OH-rich topaz.

The aqueous part of Type II fluid inclusions freezes (T_f) between −70 and −58°C (Table 3). The first melting is observed between −54 and −42°C, close to the eutectic of the NaCl–$CaCl_2$–H_2O system (Fig. 5a). This result implies that divalent ions, notably Ca^{2+}, may be present in solution. Hydrohalite melting ($T_{m\ Hhl}$) occurs in the range of −35·1 to −25·3°C (mean at −32·3°C), and the $T_{m\ ice}$ varies from −19·0 to −7·1°C (mean at −13·0°C). The carbonic part of Type II fluid inclusions melts instantaneously at temperatures ($T_{m\ CO2}$) very close to the pure CO_2 triple point (−56·6°C). The $T_{h\ CO2}$ are reported in Fig. 5b and scatter between −7·7 and 31·0°C. Commonly CO_2 homogenizes to the liquid (L + V → L), but both homogenization into the vapor (L + V → V) and critical homogenization (L + V → C) have also been measured. The total homogenization ($L_{CO2} + L_{brine}$ → homogeneous fluid), and the dissolution of daughter phases could not be measured, as inclusions decrepitate during heating.

Secondary fluid inclusions in matrix quartz: Na-rich brines (Type III), CO_2 (Type IV) and low-salinity H_2O (Type V) inclusions

In matrix quartz, three distinct populations of fluid inclusions coexist. These inclusions have different compositions and represent distinct fluid trapping events.

Type III aqueous fluid inclusions are limited to short intragranular trails extending from kyanite and OH-rich topaz (Fig. 3f). They are biphase (L + V) aqueous inclusions with a degree of filling [d_f = L/(L + V)] equal to 0·90–0·95. Inclusions (3–15 μm in size) commonly show evidence for partial decrepitation. Figure 6a shows the range of freezing and melting temperatures for Type III fluid inclusions. T_f is between −38 and −35°C, $T_{e\ H2O}$ varies from −35 to −28°C. These temperatures point to the presence of Mg^{2+} and/or Fe^{2+} ions, which have eutectics in the range of −38 to −35°C. $T_{m\ Hhl}$ is recorded between −24·8 and −19·0°C (mean at −23·3°C), and $T_{m\ ice}$ varies between −7·6 and −4·8°C

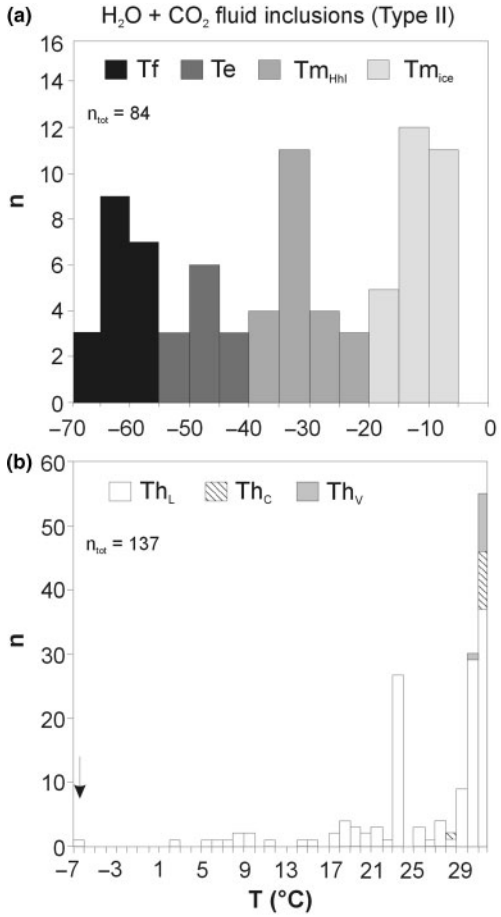

Fig. 5. Histograms for Type II fluid inclusions in OH-rich topaz: (a) H_2O freezing (T_f), eutectic (T_e), and melting (T_m) temperatures; (b) CO_2 homogenization temperatures (T_h). The arrow shows the value selected to calculate the isochore reported in Fig. 8.

(mean at −7·4°C). The $T_{h\ LH2O}$ varies from 101·5 to 259·5°C and makes a symmetric histogram with a peak at around 190°C (Fig. 6b).

Rare Type IV CO_2 fluid inclusions are present as intragranular trails within matrix quartz (Fig. 3g). These are high-density single-phase CO_2 (L) inclusions (1–10 μm in size) with polygonal contours, which suggest re-equilibration after trapping in the quartz. Evidence for partial decrepitation is common. Timing relationships between Type IV CO_2 inclusions and Type III aqueous inclusions are based on the observation of a few trails of Type IV inclusions cutting Type III inclusions. Initial melting of CO_2 is recorded at −56·8 to −56·9°C (Table 3), and final melting occurs at −56·7°C. Raman analyses show traces of N_2 (<0·1 mol%). The $T_{h\ LCO2}$ values, between −4·4 and 9·5°C (Fig. 6e), are strongly asymmetric, with most measurements around 7·4°C.

Type V liquid-rich biphase (L+V) aqueous inclusions (1–5 μm) postdate all other inclusion types and are identified as intergranular trails, locally deformed, within matrix quartz (Fig. 3h). Inclusions freeze (T_f) between −36 and −32°C, whereas T_e are between −23 and −21°C, close to the eutectic temperature of the NaCl–H_2O system. $T_{m\ ice}$ varies from −6·5 to −4·7°C (mean at −5·9°C), corresponding to 7·5–9·9 (mean = 9·1) NaCl wt % (Fig. 6c). $T_{h\ LH2O}$ ranges from 102·3 to 222·3°C, and makes an asymmetric histogram (Fig. 6d).

Fluid composition and density calculation

In Type I primary inclusions, paragonite, muscovite, anhydrite and 'alunite' represent the daughter minerals precipitated from the originally trapped fluid, as indicated by their ubiquitous presence and constant volumetric ratios. The constant relative volume proportions of these phases within inclusions show that the fluid was homogeneous at the time of trapping. The average bulk composition of the inclusions is: 30 wt % Al_2O_3, 24 wt % SiO_2, 11 wt % SO_3, 9 wt % CaO, 5 wt % K_2O, 3 wt % Na_2O, with minimum amounts of TiO_2, Fe_2O_3, FeO, MgO, BaO, P_2O_5, and $(CO_3)^{2-}$ (Ferrando *et al.*, 2005*a*). The minimum calculated water content is 20–25 wt %, based on the volume of empty cavities in inclusions, which is, however, certainly underestimated, and consequently only a proxy for the original water contents. During decompression at high pressures, selective removal of water from the fluid inclusions is a very common process, which may occur by fluid-inclusion decrepitation, leakage through dislocations, H_2 diffusion, and chemical reactions with host minerals at low temperature (Touret & Frezzotti, 2003). Presence of diaspore within the inclusions, however, indicates that liquid water was present at HP, and reacted with corundum to produce diaspore, during the exhumation of the host rocks.

Although the obtained compositions can only approximate those of the originally trapped fluids, they provide important constraints on the chemical nature of the fluids evolved during peak metamorphic conditions: (1) fluids are aqueous and contain high solute contents; (2) the dominant solutes are Si, Al, S, Ca, K and Na, whereas Mg and Fe are virtually absent; (3) Cl-ligands are negligible.

The calculated composition for preserved Type II inclusions is $X_{H2O} = 0{\cdot}87$, $X_{CO2} = 0{\cdot}04$, $X_{salt} = 0{\cdot}9$; the aqueous part of the fluid is Ca-rich brine containing 14–15 $CaCl_2$ and 2·5–3·5 NaCl in wt %. The presence of anhydrite and gypsum as daughter phases in some inclusions is consistent with a Ca-dominated solution, and further indicates that $(SO_4)^{2-}$ and $(HSO_4)^-$ represent important anions. A few of the smallest inclusions have an extremely high density (up to 1·16 g/cm^3), indicating that the original fluid inclusion densities may be locally preserved in topaz, despite a remarkable pressure differential during decompression. Re-equilibrated Type II inclusions have a considerably lower density (0·76 g/cm^3) and H_2O/CO_2 ratios ($X_{H2O} = 0{\cdot}86$, $X_{CO2} = 0{\cdot}07$, $X_{NaCl} = 0{\cdot}07$), which suggest that stretching at high temperatures and selective water

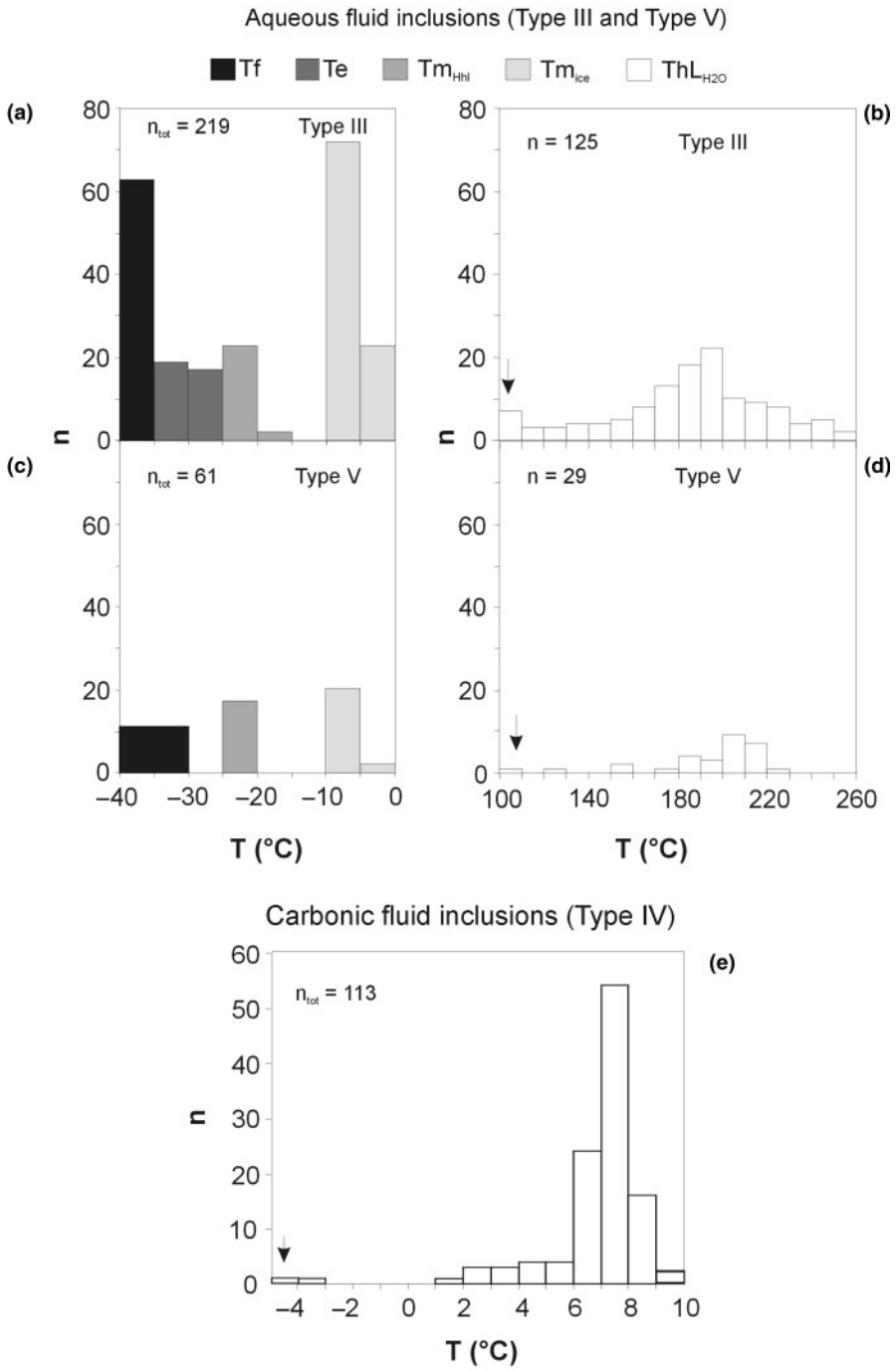

Fig. 6. Histograms for Type III, Type IV, and Type V fluid inclusions: (a) and (c) show freezing (T_f), eutectic (T_e), and melting (T_m) temperatures for Type III and V aqueous fluid inclusions; (b) and (d) show homogenization temperatures (T_h) for Type III and V aqueous fluid inclusions; (e) T_h values for Type IV CO_2 fluid inclusions. The arrows show the values selected to calculate the isochores reported in Fig. 8.

loss (Bakker & Jansen, 1990) might have been the main re-equilibration process for primary inclusions in OH-rich topaz during decompression.

Type III aqueous inclusions in matrix quartz are NaCl-rich fluids, containing one or more divalent cations. As inclusions freeze at temperatures above the eutectic of the NaCl–$CaCl_2$–H_2O system, we conclude that $CaCl_2$ is not significant in the solution. In terms of the NaCl–$MgCl_2$–H_2O system, taken as representative for solutions with a eutectic in the observed temperature range, average salinity is 4·5 NaCl wt %, and 6·5 in $MgCl_2$ equiv. wt % (Bakker, 2003). Extreme caution,

Table 4: Isotopic compositions of hydrogen and oxygen in the quartzite and temperature estimates

Sample	δD (‰)		$\delta^{18}O_{VSMOW}$ of minerals (‰)				Mineral–mineral fractionations			Temperature (°C)		
	Toz	Ms	Qtz	Ky	Toz	Rt	Qtz–Ky	Qtz–Toz	Qtz–Rt	Qtz–Ky	Qtz–Toz	Qtz–Rt
RPC 542			0.1	−2.0		−6.4	2.1		6.4	770 ± 20		610 ± 10
RPC 544		−130	0.2	−2.1			2.3			710 ± 20		
RPC 546	−60	−100	0.1	−1.3	−1.7	−6.4	1.4	1.8	6.3	980 ± 30	705 ± 30	620 ± 20
RPC 547	−82	−115	−0.3	−1.8	−1.8	−6.4	1.5	1.5	6.1	950 ± 30	780 ± 30	630 ± 20

Typically, estimates based on the Qtz–Rt fractionation yield low temperatures (e.g. Sharp, 1995; Zheng *et al.*, 1998).

however, should be taken when considering the nature of the divalent cations present in Type III inclusions, as Mg^{2+} should be present only at very low concentrations, much smaller than those of Fe^{2+} and Mn^{2+} in similar rock-equilibrated fluids. The fluid density has been calculated using the minimum $T_{h\ LH2O}$, yielding values of 1·02 g/cm^3.

Type IV fluid inclusions contain CO_2 with traces of N_2 with a maximum density of 0·93 g/cm^3. Such a value represents the minimum possible density of trapped fluids. Indeed, the widespread re-equilibration features observed in inclusions strongly suggest that all fluid densities might have been reset to lower values.

Type V aqueous fluid inclusions represent the latest trapped fluids in the studied rocks. They are NaCl solutions with a salinity between 7·5 and 10 NaCl wt %, and a density of 1 g/cm^3.

OXYGEN AND HYDROGEN ISOTOPES

The low $\delta^{18}O$ values of the minerals separated from the Sulu OH-rich topaz–kyanite quartzite ($-0{\cdot}3‰ < \delta^{18}O_{Qtz} < 0{\cdot}2‰$; $-2{\cdot}1‰ < \delta^{18}O_{Ky} < -1{\cdot}3‰$; $\delta^{18}O_{OH\text{-}Toz} = -1{\cdot}8$ and $-1{\cdot}7‰$; $\delta^{18}O_{Rt} = -6{\cdot}4‰$) are similar to those reported by Rumble & Yui (1998), and significantly lower than values expected for unaltered metapelitic rocks having undergone high-grade metamorphism. The complete dataset is reported in Table 4. The δD values of OH-rich topaz and muscovite are $-70 \pm 12‰$ and $-115 \pm 15‰$, respectively, which are also similar to the δD values reported for hydrous silicates from Dabie Shan (Zheng *et al.*, 1998, 1999; Xiao *et al.*, 2002). The $\delta^{18}O_{Toz}$ and δD_{Toz} values are the first reported for this HP phase, and the large scatter in the δD values probably results from the partial destabilization of the selected minerals (i.e. Fig. 2d: typically paragonite or pyrophyllite-mantled muscovite; Fig. 2e: paragonite flakes around OH-rich topaz). The isotope data for the minerals indicate that the UHP rocks from the Dabie–Sulu orogen are characterized by anomalously low oxygen and hydrogen isotope ratios and that the protoliths underwent meteoric–hydrothermal alteration before UHP metamorphism occurred (e.g. Zheng *et al.*, 2003).

The $^{18}O/^{16}O$ ratios decrease as follows: quartz > kyanite ≥ OH-rich topaz > rutile, as expected for equilibrium fractionation (Zheng, 1993*a*, 1993*b*), and suggest that the rocks experienced either (1) negligible open-system retrograde metamorphism, or (2) infiltration of a low $\delta^{18}O$ fluid, which did not alter significantly the peak metamorphic O-isotope composition.

Because of the refractory nature of the Al_2SiO_5 polymorphs to diffusional exchange upon cooling, even at high P–T metamorphic conditions (Fortier & Giletti, 1989; Young, 1993), oxygen isotope geothermometry provides accurate temperature estimates in alumino-silicate-bearing rocks that cooled under anhydrous conditions (Ghent & Valley, 1998; Moecher & Sharp, 1999; Vannay *et al.*, 1999; Putlitz *et al.*, 2002). Using the equation $1000 \ln \alpha = a \times 10^6/T^2$ (where α is the fractionation factor related to the temperature $= (1000 + \delta^{18}O_{phaseA})/(1000 + \delta^{18}O_{phaseB})$, O-isotope based temperatures were estimated for the following mineral pairs: Qtz–Ky ($a_{(Qtz\text{–}Ky)} = 2{\cdot}25 \pm 0{\cdot}2$; Sharp, 1995), Qtz–Toz ($a_{(Qtz\text{–}Toz)} = 2{\cdot}25 \pm 0{\cdot}2$; Zheng, 1993*a*, 1993*b*), and Qtz–Rt ($a_{(Qtz\text{–}Rt)} = 5{\cdot}02$; Matthews, 1994). At peak metamorphic conditions (stage A) the stable SiO_2 polymorph was coesite; this was transformed into quartz during the stage B transition. The calculated temperature may be slightly lower than the original one because of pressure effects, which have been estimated to be of the order of 40°C at 4 GPa (Sharp *et al.*, 1992).

Oxygen isotope thermometry was combined with the conventional 'cation-based' thermometric estimates for other rocks in the same area, to constrain the metamorphic conditions of the Sulu quartzites and to reconstruct the metamorphic evolution of this terrane (see following paragraph).

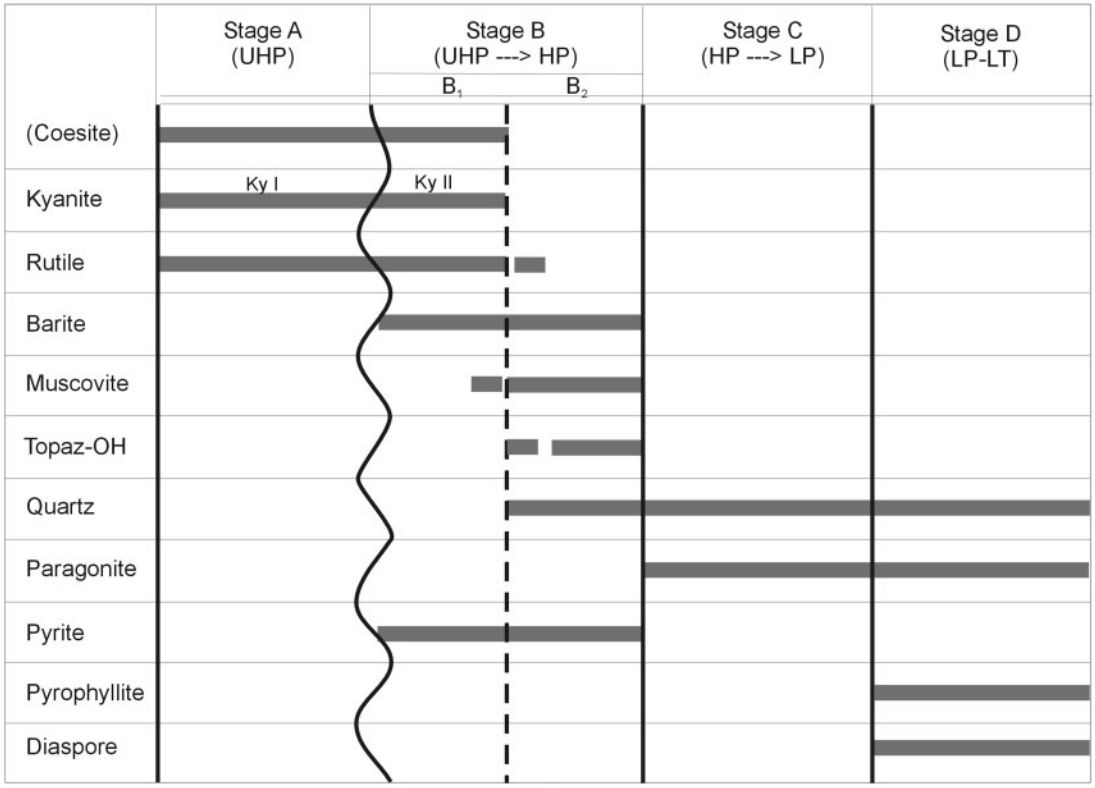

Fig. 7. Metamorphic evolution of the Hushan OH-rich topaz–kyanite quartzites.

DISCUSSION

Metamorphic evolution

Although the studied quartzites show a relatively simple mineralogy, the scarce evidence of retrogression allows us to reconstruct the polyphase metamorphic evolution, summarized in Fig. 7. A P–T path characterized by four metamorphic stages—from the metamorphic peak to the late stages of exhumation—is shown in Fig. 8, combining microstructural relationships, mineralogical compatibilities, fluid inclusion isochores, stable isotope geothermometry, and theoretical phase relationships. The petrogenetic grid is based on selected phase relationships in the Na_2O–K_2O–Al_2O_3–SiO_2–H_2O–CO_2 (NKASCH) system with excess SiO_2, calculated with the thermodynamic approach of Connolly (1990), using a modified 'internally consistent' thermodynamic database of Holland & Powell (1998). All equilibrium curves are calculated for $a_{H2O} = 1$, except for those involving paragonite, and OH-rich topaz. The curve for the reaction Pg = Ky + Jd + fluid at $a_{H2O} = 0{\cdot}75$ is extrapolated from the experiments of Tropper & Manning (2004). The isopleth for the reaction Al-silicate + fluid = Toz is calculated considering a topaz with $X_{OH} = 0{\cdot}30$ (i.e. close to $X_{OH} = 0{\cdot}28$, obtained from WDS and X-ray diffraction analyses of topaz), and a H_2O–NaCl–CO_2 fluid phase with $X_{H2O} = 0{\cdot}90$ ($X_{H2O} = 0{\cdot}87$ in Type II inclusions). Thermodynamic models for low-pressure reactions involving topaz, with variable X_{OH} between 0·05 and 0·40, were developed by Barton (1982), whereas those for high-pressure reactions (Wunder *et al.*, 1993, 1999), are restricted to topaz with $X_{OH} = 1$. To obtain the isopleth for topaz with $X_{OH} = 0{\cdot}30$, the thermodynamic database of Holland & Powell (1998) has been modified by the insertion of thermodynamic data for a topaz with $X_{OH} = 0{\cdot}30$ following the model proposed by Barton (1982) for the hydroxyl-topaz in solid solution with fluor-topaz, i.e. $a_{Toz} = (X_{OH})^2$. The dry melting curve for Ms, with excess SiO_2, to give Ky + liquid (L) is from Huang & Wyllie (1973), whereas the equilibrium curve involving diamond is from Bundy (1980). The calculated isochores for Type II, III, IV and V fluids, and the geothermometry by oxygen isotopes are also shown (Fig. 8).

The bulk chemical composition of the quartzite suggests a sedimentary protolith, such as a clay-rich sandstone (see also Zhang *et al.*, 2000, 2005*a*). Rare quartz or very fine-grained zircon crystals within Ky I preserve a folded pre-peak foliation, yet their occurrence is not sufficient to estimate the prograde P–T conditions.

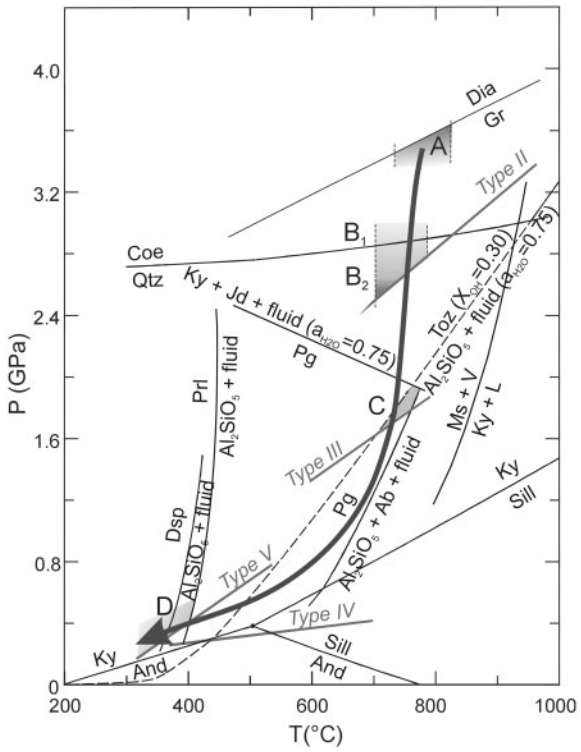

Fig. 8. Pressure–temperature (P–T) diagram showing the metamorphic evolution stages (A–D) of OH-rich topaz–kyanite quartzites. The petrogenetic grid, based on selected phase relationships in the NKASCH system with excess SiO_2, was calculated with the thermodynamic approach of Connolly (1990) and the modified database of Holland & Powell (1998). The curve for the reaction Pg = Ky + Jd + fluid at $a_{H2O} = 0{\cdot}75$ is extrapolated from Tropper & Manning (2004). The curves involving muscovite and diamond are from Huang & Wyllie (1973) and Bundy (1980), respectively. Fields labeled A–D refer to the main metamorphic stages shown in Fig. 7. Vertical dashed lines are oxygen geothermometric estimates. The grey bands are the isochores determined from microthermometric data for Type II, III, IV, and V fluid inclusions, respectively.

The peak metamorphic stage (A in Fig. 8) is represented by the anhydrous assemblage Ky I + coesite + rutile. Temperatures calculated from the $\delta^{18}O$ values of quartz and kyanite ($\Delta^{18}O_{Qtz-Ky}$) in Toz-free samples are 730–820°C (Table 4). At these temperatures, the occurrence of coesite and the absence of diamond constrain pressures conditions between 2·9 and 3·5 GPa. These pressure conditions are in agreement with those obtained from nearby eclogites (3·5–4·0 GPa, Ferrando *et al.* 2005*b*). In contrast, O-isotope thermometry on Ms- and Toz-bearing samples RPC 546 and RPC 547 yields temperatures of 980 ± 30°C and 950 ± 100°C, respectively, which are not geologically plausible for the Donghai area. These T estimates probably result from O-isotope disequilibrium between quartz and Kyanite I (±Kyanite II).

The first decompression stage (stage B in Figs 7 and 8) is characterized by an earlier crystallization of Ky II (event B_1) and a later growth of hydrous phases (event B_2). OH-rich topaz possibly formed by the reaction Ky + fluid = Toz, similar to that invoked for the prograde Ky–Toz breakdown. For this reason, the transition from anhydrous (event B_1) to hydrous (event B_2) minerals during stage B is more probably related to an increase in the water activity rather than to a pronounced variation in the P–T conditions. Probably, the water entered the quartzite at the coesite–quartz transition, promoted by the volume change that accompanies this reaction.

The $\delta^{18}O$ value of kyanite, measured in Toz-bearing samples, possibly results from the combination of $\delta^{18}O_{KyI}$ and $\delta^{18}O_{KyII}$, or more probably (mainly coarse-grained minerals were hand-picked), from the $\delta^{18}O$ value of Kyanite I acquired during hydration at the early decompression stage. It is worth noting that oxygen isotope geothermometry based on the Qtz–Toz pair constrains temperature conditions for metamorphic stage B at 705–780°C (Table 4), matching the temperature estimates based on the Qtz–Ky pair in Toz-free rocks. The fluid isochore, obtained from the extremely high-density Type II brines (1·16 g/cm^3), indicates a pressure of 2·7 GPa, and locates stage B at the coesite–quartz transition (Fig. 8). The P–T estimates indicate a near-isothermal decompression, as inferred from the observed metamorphic parageneses.

Calculated P–T conditions for topaz growth are close to those proposed by Zhang *et al.* (2002) for prograde-peak OH-rich topaz from Fushan (700°C and 2·8 GPa). However, in our samples textural evidence clearly indicates that topaz is retrograde and replaces UHP peak Ky I, excluding the growth of topaz during stage A. Since the stability of the F–OH topaz solid solution is defined by P, T, OH content, and a_{H2O} in the fluid phase, the absence of OH-rich topaz at the metamorphic peak may be explained by a variable water activity during the metamorphic evolution. As the equilibrium curves for the reaction Al-silicate + fluid = Toz, in the presence of a fluid phase with $a_{H2O} < 1$, are not known, we have calculated a petrogenetic grid (Fig. 9), which shows some of the variations of the stability field of OH-topaz ($X_{OH} = 0{\cdot}30$) for different water activities in the fluid, using the thermodynamic approach described above. At stage B (705–780°C and 2·9 GPa), the water activity in Type II brines has been calculated at about 0·75 (Aranovich & Newton, 1999) and is consistent with the stability of topaz. Based on Fig. 9, during stage A at UHP conditions (730–820°C and 2·9–3·5 GPa), fluid water activity was low, and ≤0·4, to maintain the anhydrous assemblage Ky + Coe. At higher water contents, OH-rich topaz would have been the stable phase, instead of kyanite.

Stage C (Fig. 8) is characterized by growth of paragonite after both kyanite and OH-rich topaz, and by recrystallization of matrix quartz. In particular, both the

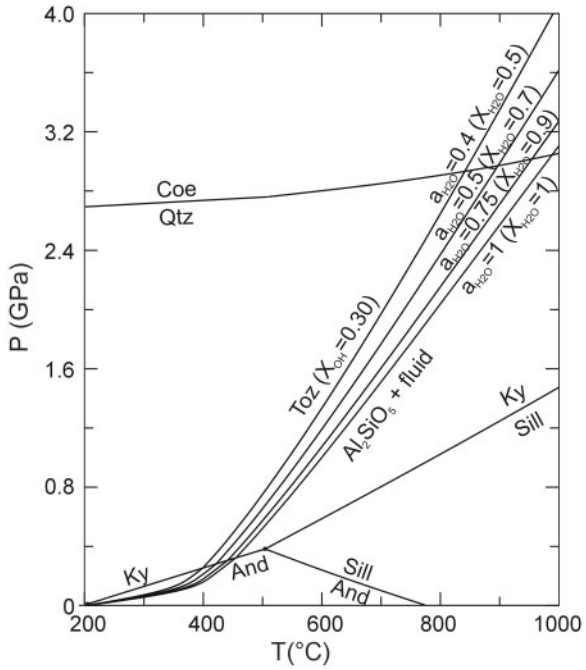

Fig. 9. Pressure and temperature variation of the stability field of topaz with $X_{OH} = 0{\cdot}30$ in the presence of fluids with different water activity (i.e. H_2O and variable amounts of CO_2 and/or salts). The petrogenetic grid, based on selected phase relationships in the Al_2O_3–SiO_2–CO_2–H_2O (ASCH) system with excess SiO_2, was calculated with the thermodynamic approach of Connolly (1990) and the modified database of Holland & Powell (1998).

destabilization of the OH-rich topaz and the crystallization of paragonite constrain the temperatures to values between 700 and 780°C [curves Toz ($X_{OH} = 0{\cdot}30$) = Al-silicate + fluid, and Pg = Al-silicate + Ab + fluid, in Fig. 8]. A minimum pressure of 1·6 GPa is obtained from Type III fluid isochores, and 1·9 GPa is calculated from the curve of destabilization of kyanite (Fig. 8; Ky + Jd + fluid = Pg at $a_{H2O} = 0{\cdot}75$; Tropper & Manning, 2004). The last stage of retrogression (stage D in Fig. 8) is characterized by the growth of pyrophyllite and diaspore after kyanite. The reactions Ky + fluid = Prl and Ky + fluid = Dsp indicate retrograde temperatures lower than 410°C and 370°C, respectively. Pressure conditions of about 0·3 GPa, consistent with greenschist-facies conditions, are obtained by the fluid isochore calculated for Type V fluid inclusions.

The reconstructed P–T path shows that the quartzites are characterized by a UHP peak, strong near-isothermal decompression from UHP to HP conditions, and almost isobaric cooling from amphibolite- to greenschist-facies conditions (Fig. 8), similar to P–T paths for eclogite reported in previous studies of the Donghai area (e.g. Zhang *et al.*, 1995; Hirajima & Nakamura, 2003; Ferrando *et al.*, 2005b; Zhang *et al.*, 2005*a*). Finally, the reconstructed P–T metamorphic evolution demonstrates that combined stable isotope geothermometry and fluid inclusion isochores may be a viable alternative to cation geothermobarometry in UHP–HP rocks characterized by unfavorable mineral assemblages.

Nature of fluid phases evolved at UHP and HP, and fluid–rock interaction

Fluids at UHP conditions: alkali-alumino-silicate aqueous solutions, intermediate between an aqueous fluid and a hydrous melt

The presence of primary Type I multiphase solid inclusions in peak Ky I indicates that the dominant peak mineral association of kyanite and coesite at 3·5 GPa and 730–820°C was formed in the presenc of a hydrous fluid phase in the quartzites. Peak aqueous fluids contain high amounts of Al, Si, S, Ca, Na, and K (Fig. 10). Conversely, ligands such as Cl seem to be irrelevant, and the rarity of carbonates indicates a very subordinate role for CO_2 as well. The calculated range of Type I fluid water content, although speculative, is >25 and ≤48 wt %: the minimum value has been derived from Type I inclusions, and the maximum value has been calculated based on the stability field of OH-topaz derived from phase equilibria (see Figs 9 and 10).

The first remarkable feature of deep Type I fluids is represented by the dominant alkali–alumino-silicate (-sulfate) character of the solutes. This composition is different from the Cl-rich brines reported at peak conditions in other HP and UHP rocks from Sulu and other localities (Philippot & Selverstone, 1991; Selverstone *et al.*, 1992; Svensen *et al.*, 1999; Fu *et al.*, 2003; Zhang *et al.*, 2005*b*, 2006; Xiao *et al.*, 2006). In addition, Type I fluids are highly concentrated, resulting in an unusual composition, which is intermediate between a fluid and a melt. However, it is highly improbable that these fluids represent remnants of a water-rich silicate melt trapped as inclusions in peak kyanite. Based on previous experimental studies in metapelites, muscovite (e.g. phengite) is the major hydrous mineral potentially involved in melting at $P > 3$ GPa. In phengite-dominated melting, first melts are potassic high-silica rhyolites (Schmidt *et al.*, 2004, and references therein). Type I fluids do not have, or even approximate, a rhyolitic composition, as they are too poor in SiO_2, and too rich in Al_2O_3, CaO, and SO_3. Furthermore, calculated water contents of Type I fluids are too high for a silicate melt, as the maximum water dissolved in a melt at the considered pressures cannot exceed 25–30 wt % (Kennedy *et al.*, 1962; Boettcher & Wyllie, 1969).

None of the obtained compositions could result from selective major oxide enrichments during retrograde inclusion evolution (see Frezzotti, 2001). There is, in fact, no evidence for chemical interaction with the host kyanite (Ferrando *et al.*, 2005*a*), and even if crystallization of the

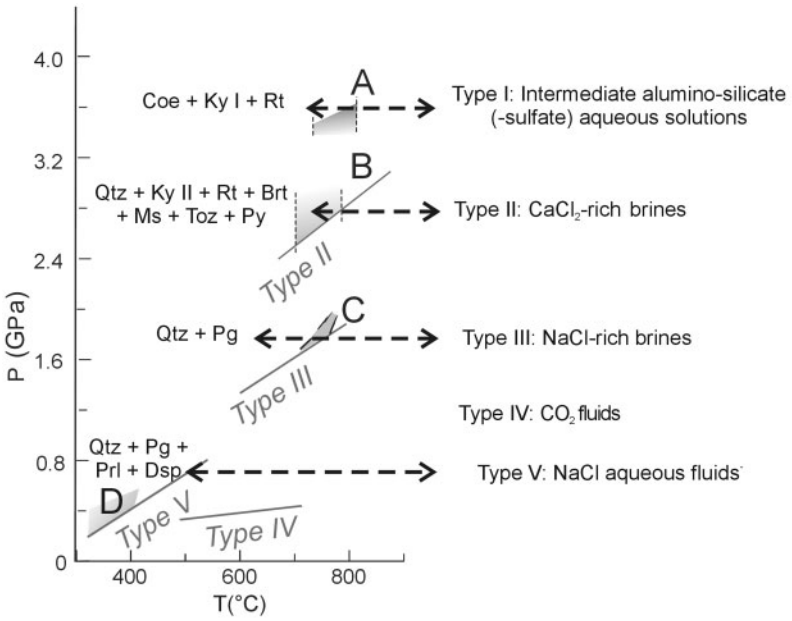

Estimated compositions of aqueous fluids

Fluid	P	T	X_{H2O}	X_{CO2}	Solutes wt%								H_2O	a_{H2O}
Type	GPa	°C			Si^{4+}	Al^{3+}	Ca^{2+}	Mg^{2+}	Na	K	SO_4^{2-}	Cl^-	wt%	
I	3.5	780	0.60	-	11.2	15.6	6.5	<1	2.2	4.1	11	-	48	0.40
II	2.9	740	0.87	0.08	-	-	5.4	n.a.	1.7	n.a.	0-4	11.9	82	0.75
III	1.6	740	0.95	-	-	-	-	1.7	1.8	n.a.	-	7.5	89	0.92
V	0.3	400	0.95	-	-	-	-	-	4	n.a.	-	6.0	90	0.92

Fig. 10. Proposed schematic fluid–rock interaction in OH-rich topaz–kyanite quartzite from Hushan, reporting the chemistry of each fluid type. The *P–T* evolution for the studied rocks is simplified from Fig. 8.

host kyanite occurred on the inclusion's wall, it would not modify the Al_2O_3/SiO_2 ratio of the melt.

We propose that the Type I UHP fluids represent intermediate alkali–alumino-silicate aqueous solutions (H_2O $\leq$50 wt %) at high pressures. A similar intermediate composition might indicate that fluids have evolved at pressures above the critical curve of the silicate–H_2O system; that is, their composition reflects supercritical hydrous silicate liquids (Stalder *et al.*, 2000; Kessel *et al.*, 2005). The *P–T* conditions of the second critical end-point on the melting curve strongly depend on the nature of the silicate–H_2O systems, ranging from 1 to >12 GPa, from silica-rich to mafic and ultramafic compositions (Kennedy *et al.*, 1962; Anderson & Burnham, 1965; Eggler & Rosenhauer, 1978; Ryabchikov, 1993; Mysen, 1998; Bureau & Keppler, 1999; Stalder *et al.*, 2000, 2001). In the simple NASH system, Bureau & Keppler (1999) have demonstrated that critical conditions might be attained at pressure as low as 1·6 GPa, and experimental results in natural granitic rocks indicate pressures of 2·0–2·6 GPa (Schreyer, 1999; Kawamoto, 2004). In general, the increase in Mg, Fe, K, and Ca contents greatly raises the pressure of the second critical point, whereas addition of volatile elements, such as B and F, has the opposite effect (Thomas *et al.*, 2000; Sowerby & Keppler, 2002).

It is not known where the intersection between the critical curve and the H_2O-saturated solidus lies, or even the existence of a system relevant to this bulk composition (note, however, that an end point need not exist for the fluid or liquid to be supercritical).

The existence of an intermediate fluid (H_2O $\leq$50 wt %) enriched in Al, Si, S, Ca, K, and Na, leads us to propose that at 3–3·5 GPa and 780°C rocks in the (NK)ASH system may generate fluids of intermediate composition, which are at supercritical conditions.

Fluid alkali–alumino-silicate components mirror the bulk composition of the host rock, and suggest that Type I intermediate solutions may have been formed by progressive dehydration of muscovite ± paragonite during prograde and UHP peak metamorphism. To be really effective this process must have acted on a small volume of fluid locally, trending towards increasing solute content and a heterogeneous distribution of fluids. As Type I intermediate solutions are internally derived, we may speculate

that they were ultimately (indirectly, via hydro-silicate breakdown) derived from the meteoric–hydrothermal event. This observation has been recently inferred also on the basis of a Fourier transform infrared investigation in nominally anhydrous minerals from Dabie-Shan eclogites (Xia *et al.*, 2005).

Fluids at the transition from UHP to HP conditions: $CaCl_2$ brines

The earliest isothermal decompression stages, at the transition from UHP to HP conditions (2·9 GPa and 705–780°C), led to a progressive growth of hydrated phases (such as muscovite and OH-rich topaz), and of minor barite and pyrite. Type II fluid inclusions indicate that OH-rich topaz grew from a Ca-rich Cl and $(SO_4)^{2-}$ brine, where Si and Al are virtually absent (Fig. 10). Muscovite does not contain fluid inclusions, but it probably grew in the presence of the same fluid. The brines include traces of CO_2 and should also have contained F, accommodated in both topaz and muscovite. Total fluid salinity is 18–20 in NaCl equiv. wt % as indicated by the Type II inclusions, which have preserved the original densities.

Assuming that silica, alumina and K_2O were consumed during the growth of both muscovite and topaz, then the nature of most of the solutes present in Type II fluids is close to that of Type I intermediate solutions. Two major differences, however, are observed (Fig. 10): the presence of high amounts of Cl (12 wt %), and a sharp increase in the water content (82 wt % H_2O). An evolution in a closed fluid system could not account for the observed variations in fluid chemistry. If, in fact, lowering of solubility as a result of decompression led to selective precipitation of a large part of the solutes from Type I fluids, initiating the growth of muscovite and OH-rich topaz, it seems unlikely that this represents the only process responsible for the observed increase of water activity. Most importantly, as much as 12 wt % Cl is present in Type II brines, which cannot be derived from Type I fluids because these do not contain significant chlorine.

In Sulu UHP rocks, similar HP $CaCl_2$-rich brines are commonly observed in both low and high $\delta^{18}O$ rocks (Fu *et al.*, 2003; Xiao *et al.*, 2006). These brines are, therefore, unrelated to the O-isotope composition of UHP rocks, as expected for remnants of internally derived UHP and/or HP fluids. In the studied rocks, brines are present within topaz-bearing quartzite, whereas they are absent in topaz-free domains. As mentioned above, the paragenetic minerals from the topaz-bearing rocks show low $\delta^{18}O$ values similar to those of the topaz-free samples; however, quartz and Ky I from these domains are not in O-isotope equilibrium, as defined by unrealistic thermometric estimates, whereas O-isotope equilibrium is preserved in topaz-free rocks (Table 4). This observation clearly indicates that topaz-bearing domains were infiltrated by low-^{18}O fluids, which are similar in O-isotope composition to the low-^{18}O quartzites, although slightly higher. These necessarily external (Cl-rich) fluids infiltrated the quartzites upon topaz crystallization, thus after the UHP metamorphic peak.

If the new $\delta^{18}O_{ky}$ results from external fluid infiltration, it may be qualitatively used to infer the water/rock (W/R) ratios in the topaz-bearing domains upon fluid infiltration according to the mass-balance equation

$$W/R = \frac{\delta^{18}O^{f}_{ky} - \delta^{18}O^{i}_{ky}}{\delta^{18}O^{i}_{W}} - \left[\delta^{18}O^{f}_{ky} - \Delta_{ky-H_2O}\right]$$

where $\delta^{18}O^{f}_{ky}$ is the $\delta^{18}O_{ky}$ of topaz-bearing domains, $\delta^{18}O^{i}_{ky}$ is the $\delta^{18}O_{ky}$ of topaz-free domains, $\delta^{18}O^{i}_{W}$ is the O-isotope composition of the infiltrating fluid and Δ_{ky-H_2O} is the isotopic fractionation between kyanite and water, that is $-0{\cdot}90$ at $T = 700°C$ (Zheng, 1993*a*). Because the Δ_{ky-H_2O} is negative, the $\delta^{18}O^{i}_{W}$ needs to be >0‰. For a Δ_{ky-H_2O} value between zero and +2‰ the resulting W/R ratios range from 1·8 to 0·3. These W/R ratios should be considered minimum values, because the water is assumed to have reacted completely with the rock.

The W/R values do not change significantly if an open-system infiltration model is assumed ($= \ln[W/R_{closed} + 1]$). It could be argued that the zero-dimensional model, which describes the simple mass-balance calculation used to estimate the W/R ratio, may not be adequate for a very low-porosity rock in which very low amounts of fluids entered during exhumation from UHP to HP conditions. What should be pointed out, however, is that at least discrete amounts of $CaCl_2$-rich brines with higher $\delta^{18}O$ values entered the quartzite rock system during the early stages of decompression, indicating that the retrograde fluid–rock interaction locally occurred in a open system, probably generated at the coesite–quartz inversion. Brines probably originated from the mafic and ultramafic eclogitic rocks adjacent to the quartzites, where they have been recognized as dominant UHP and HP fluids (Xiao *et al.*, 2000, 2001; Franz *et al.*, 2001; Fu *et al.*, 2001, 2003; Zhang *et al.*, 2006).

Fluids at HP conditions: NaCl brines ± CO_2

The final stages of the exhumation history preserve at least three distinct events of limited fluid flow within the quartzites. Fluid compositions were constrained by Na-rich brines with higher water activities (Type III), followed by minor pure CO_2 fluids (Type IV), and by late low-salinity brines (Type V) (Fig. 10). The Na-rich brines (Type III) were present during the events that resulted in the growth of paragonite and the recrystallization of quartz at pressures below 2 GPa: their Na-rich nature may account for the onset of paragonite crystallization after both kyanite

and topaz. Type III fluids are distinctly different from Type II brines (Fig. 10), mostly because of the absence of Ca and lower salinity. Whether this reflects post-entrapment diffusion of elements between fluid inclusions and host mineral, or initial geochemical differences is not clear. Despite the lack of petrographic evidence for the formation of calcite and/or gypsum by retrograde reactions in the rock, a decrease in Ca solubility is still a plausible mechanism to explain the disappearance of Ca from the fluid at lower pressure conditions.

CO_2 fluids (Type IV) are rare and do not show any microstructural indication for heterogeneous trapping in inclusions along with Type III brines, excluding the possibility that CO_2 might represent an immiscible fluid phase coeval with Type III brines. The distribution of CO_2 inclusions suggests that their formation occurred at a later stage (Fig. 10). CO_2 fluids are rather common late-stage fluids in UHP rocks from Dabie–Sulu. The general interpretation is that CO_2 is external in origin and possibly locally derived from granulites (Touret, 2001; Touret & Frezzotti, 2003).

The last fluid event at greenschist-facies conditions is characterized by the presence of rare aqueous fluids, which were locally trapped as Type V inclusions (Fig. 10). These fluids, very common in the latest stages of retrogression of the studied metamorphic rocks, promote the growth of late hydrous minerals, such as pyrophyllite and diaspore, in the most retrogressed samples.

CONCLUSIONS

OH-rich topaz–kyanite quartzites from the Sulu UHP metamorphic terrane are characterized by an anhydrous peak mineral assemblage that formed at 730–820°C and 2·9–3·5 GPa in the presence of intermediate fluids, containing significant amounts of Si, Al, SO_4, Ca, K, and Na in solution, which probably represent supercritical liquids. They are probably derived from dehydration reactions, occurring during prograde and peak metamorphism, at UHP conditions. Peak alkali–alumino-silicate solutions are oxidized (sulfur present as sulfate) and do not contain significant CO_2. Oxidized conditions and absence of CO_2 might explain the extreme scarcity of micro-diamond in this area.

During early decompression, at the transition from UHP to HP conditions (2·9 GPa and 705–780°C), fluids are characterized by a high $CaCl_2$ content, and by a sharp increase in the water activity (from 0·4 to 0·75). At these conditions, muscovite and OH-rich topaz crystallized at the expense of kyanite. Increase of water activity and addition of Cl^- suggest that brines cannot have been derived from intermediate UHP solutions by decompression. Oxygen isotope data indicate discrete influx from neighboring lithologies, at the coesite–quartz transition.

Later stages at amphibolite- and greenschist-facies conditions are defined by limited circulation of Na-rich aqueous fluids. CO_2 does not seem to be an important fluid phase during the overall metamorphic evolution of these crustal rocks.

We, therefore, propose a new model for fluid–rock interaction in the deeply subducted continental lithologies of the Sulu terrane, in which intermediate alumino-silicate solutions with low water activity represent internally derived fluids at UHP conditions, and early retrograde brines correspond to an external input of Cl-rich aqueous fluids. Such a model may explain the anhydrous nature of the peak mineral assemblage, the growth of hydrated phases during early decompression, and the $\delta^{18}O$ values of rocks in this area. This study provides evidence that subducted continental lithologies may release aqueous fluids, which are rich in alkalis, Al and Si, and Cl-poor, with intermediate compositions. An important consequence is that fluids with major differences in solutes and water content may be released during UHP evolution of continental metamorphic assemblages.

ACKNOWLEDGEMENTS

Most of this research originates from the Ph.D. thesis of S.F. We acknowledge Shutong Xu, Y. Liu, W. Wu and F. Rolfo for assistance during field work. We are grateful to D. Castelli for discussion, and help in calculating the petrogenetic grid. The paper greatly benefited from reviews by C. Manning, Z. D. Sharp and an anonymous reviewer, and from editorial assistance by R. Gieré. Raman analytical facilities were provided by the Italian organization for research in Antarctica (PNRA). F. Olmi made available microprobe facilities in Firenze. This work was funded by national (MURST, CNR), and local ('Finanziamento Convenzioni Interuniversitarie', 'Fondi Scambi Culturali'—University of Torino, and 'Programmi Ricerca di Ateneo 2004'—University of Siena) grants.

REFERENCES

Alberico, A., Ferrando, S., Ivaldi, G. & Ferraris, G. (2003). X-ray single-crystal structure refinement of an OH-rich topaz from Sulu UHP terrane (Eastern China)—structural foundation of the correlation between cell parameters and fluorine content. *European Journal of Mineralogy* **15**, 875–881.

Ames, L., Zhou, G. & Xiong, B. (1996). Geochronology and isotopic character of ultrahigh-pressure metamorphism with implications for collision of the Sino-Korean and Yangtze cratons, central China. *Tectonics* **15**, 472–489.

Anderson, G. M. & Burnham, C. W. (1965). The solubility of quartz in supercritical water. *American Journal of Science* **263**, 494–511.

Antignano, G. & Manning, C. E. (2005). Rutile solubility in H_2O–$NaAlSi_3O_8$ fluids at high *T* and *P*: implications for HFSE mobility in subduction zones. *American Geophysical Union, Fall Meet. Suppl., Abstract* **86**, V31C-0620 .

Aranovich, L. Y. & Newton, R. C. (1999). Experimental determination of CO_2–H_2O activity–composition relations at 600–1000°C and

6–14 kbar by reversed decarbonation and dehydration reactions. *American Mineralogist* **84**, 1319–1332.

Bakker, R. J. (2003). Package FLUIDS 1. Computer programs for analysis of fluid inclusion data and for modelling bulk fluid properties. *Chemical Geology* **194**, 3–23.

Bakker, R. J. & Jansen, J. B. H. (1990). Preferential water leakage from fluid inclusions by means of mobile dislocations. *Nature* **345**, 58–60.

Barton, M. D. (1982). The thermodynamic properties of topaz solid solutions and some petrologic applications. *American Mineralogist* **67**, 956–974.

Boettcher, A. L. & Wyllie, P. J. (1969). The system $CaO–SiO_2–CO_2–H_2O$. III. Second critical end-point on the melting curve. *Geochimica et Cosmochimica Acta* **33**, 611–632.

Bundy, F. P. (1980). The *P*, *T* phase and reaction diagram for elemental carbon. *Journal of Geophysical Research* **85**, 6930–6936.

Bureau, H. & Keppler, H. (1999). Complete miscibility between silicate melts and hydrous fluids in the upper mantle: experimental evidence and geochemical implications. *Earth and Planetary Science Letters* **165**, 187–196.

Chopin, C. (1984). Coesite and pure pyrope in high-grade blueschists of the western Alps: a first record and some consequences. *Contributions to Mineralogy and Petrology* **86**, 107–118.

Connolly, J. A. D. (1990). Multivariable phase diagrams: an algorithm based on generalized thermodynamics. *American Journal of Science* **290**, 666–718.

Eggler, D. H. & Rosenhauer, M. (1978). CO_2 in silicate melts: II. Solubilities of CO_2 and H_2O in $CaMgSi_2O_6$ (diopside) liquids and vapors at pressures to 40 kbar. *American Journal of Science* **278**, 64–94.

Ferrando, S., Frezzotti, M. L., Dallai, L. & Compagnoni, R. (2005a). Multiphase solid inclusions in ultrahigh pressure metamorphic rocks from Su-Lu belt (China): evidence for critical silicate-rich aqueous fluids released during continental subduction. *Chemical Geology* **223**, 68–81.

Ferrando, S., Frezzotti, M. L., Dallai, L. & Compagnoni, R. (2005b). Fluid–rock interaction in UHP Phe–Ky–Ep eclogite from the Su-Lu orogen (Eastern China). *International Geology Review* **47**, 750–774.

Fortier, S. M. & Giletti, B. J. (1989). An empirical model for predicting diffusion coefficients in silicate minerals. *Science* **245**, 1481–1484.

Franz, L., Romer, R. L., Klemd, R., Schmid, R., Oberhänsli, R., Wagner, T. & Shuwen, D. (2001). Eclogite-facies quartz veins within metabasites of the Dabie Shan (eastern China): pressure–temperature–deformation path, composition of the fluid phase and fluid flow during exhumation of high-pressure rocks. *Contributions to Mineralogy and Petrology* **141**, 322–346.

Frezzotti, M. L. (2001). Silicate-melt inclusions study in magmatic rocks: applications to petrology. *Lithos* **55**, 273–299.

Fu, B., Touret, J. L. R. & Zheng, Y.-F. (2001). Fluid inclusions in coesite-bearing eclogites and jadeite quartzite at Shuanghe, Dabie Shan (China). *Journal of Metamorphic Geology* **19**, 529–545.

Fu, B., Zheng, Y.-F. & Touret, J. L. R. (2002). Petrological, isotopic and fluid inclusion studies of eclogites from Sujiahe, NW Dabie Shan (China). *Chemical Geology* **187**, 107–128.

Fu, B., Touret, J. L. R. & Zheng, Y.-F. (2003). Remnants of pre-metamorphic fluid and oxygen-isotopic signatures in eclogites and garnet clinopyroxenite from the Dabie–Sulu terranes, eastern China. *Journal of Metamorphic Geology* **21**, 561–578.

Ghent, E. D. & Valley, J. W. (1998). Oxygen isotope study of quartz–Al_2SiO_5 pairs from the Mica Creek area, British Columbia: implications for the recovery of peak metamorphic temperatures. *Journal of Metamorphic Geology* **16**, 223–230.

Guo, F., Fan, W., Wang, Y. & Zhang, M. (2004). Origin of early Cretaceous calc-alkaline lamprophyres from the Sulu orogen in eastern China: implications for enrichment processes beneath continental collision belt. *Lithos* **78**, 291–305.

Hermann, J., Spandler, C., Hack, A. & Korsakov, A. V. (2006). Aqueous fluids and hydrous melts in high-pressure and ultra-high pressure rocks: implications for element transfer in subduction zones. *Lithos* **92**, 399–417.

Hirajima, T. & Nakamura, D. (2003). The Dabie Shan–Sulu orogen. In: Carswell, D.A. & Compagnoni, R. (eds) *Ultrahigh-pressure Metamorphism: European Mineralogical Union Notes in Mineralogy, 5*. Budapest: Eötvös University Press, pp. 105–144.

Holland, T. J. B. & Powell, R. (1998). An internally consistent thermodynamic dataset for phases of petrological interest. *Journal of Metamorphic Geology* **16**, 309–343.

Huang, W. L. & Wyllie, P. J. (1973). Muscovite dehydration and melting in deep crust and subducted ocean sediments. *Earth and Planetary Science Letters* **18**, 133–136.

Kawamoto, T. (2004). Critical phenomena between magmas and aqueous fluid (in Japanese with English abstract). *Review in High Pressure Science and Technology* **14**, 235–241.

Kennedy, G. C., Wasserburg, G. J., Heard, H. C. & Newton, R. C. (1962). The upper three-phase region in the system $SiO_2–H_2O$. *American Journal of Science* **260**, 501–521.

Kessel, R., Schmidt, M. W., Ulmer, P. & Pettke, T. (2005). The trace element signature of subduction zone fluids, melts and supercritical liquids at 120–180 km depth. *Nature* **437**, 724–727.

Kretz, R. (1983). Symbols for rock-forming minerals. *American Mineralogist* **68**, 277–279.

Li, S., Xiao, Y., Liou, D., Chen, Y., Ge, N., Zhang, Z., Sun, S., Cong, B., Zhang, R., Hart, S. R. & Wang, S. (1993). Collision of the North China and Yangtze blocks and formation of coesite-bearing eclogites: timing and processes. *Chemical Geology* **109**, 89–111.

Liu, F., Xu, Z., Katayama, I., Yang, J., Maruyama, S. & Liou, J. G. (2001). Mineral inclusions in zircons of para- and ortho-gneiss from pre-pilot drillhole CCSD-PP1, Chinese Continental Scientific Drilling Project. *Lithos* **59**, 199–215.

Liu, F., Xu, Z., Liou, J. G., Katayama, I., Masago, H., Maruyama, S. & Yang, J. (2002). Ultrahigh-pressure mineral inclusions in zircons from gneissic core samples of the Chinese Continental Scientific Drilling Site in eastern China. *European Journal of Mineralogy* **14**, 499–512.

Lu, F., Zhao, L., Deng, J. & Zheng, J. (1995). Discussion on the ages of kimberlitic magma activity in the North China platform. *Acta Petrologica Sinica* **11**, 365–374.

Manning, C. E. (2004). The chemistry of subduction-zone fluids. *Earth and Planetary Science Letters* **223**, 1–16.

Matthews, A. (1994). Oxygen-isotope geothermometers for metamorphic rocks. *Journal of Metamorphic Geology* **12**, 211–219.

Mattinson, C. G., Zhang, R. Y., Tsujimori, T. & Liou, J. G. (2004). Epidote-rich talc–kyanite–phengite eclogites, Sulu terrane, eastern China: $P–T–f_{O2}$ estimates and the significance of the epidote–talc assemblage in eclogite. *American Mineralogist* **89**, 1772–1783.

Moecher, D. P. & Sharp, Z. D. (1999). Comparison of conventional and garnet–aluminosilicate–quartz O isotope thermometry: insights for mineral equilibration in metamorphic rocks. *American Mineralogist* **84**, 1287–1303.

Mysen, B. O. (1998). Interaction between aqueous fluid and silicate melt in the pressure and temperature regime of the Earth's crust

and upper mantle. *Neues Jahrbuch für Mineralogie, Abhandlungen* **172**, 227–244.

Niggli, P. (1920). *Die leichtflüchtigen Bestandteile im Magma*. Leipzig: B. G. Teubner.

Philippot, P. & Selverstone, J. (1991). Trace-element-rich brines in eclogitic veins: implications for fluid composition and transport during subduction. *Contributions to Mineralogy and Petrology* **106**, 417–430.

Philippot, P., Chevallier, P., Chopin, C. & Dubessy, J. (1995). Fluid composition and evolution in coesite-bearing rocks (Dora–Maira massif, Western Alps): implications for element recycling during subduction. *Contributions to Mineralogy and Petrology* **121**, 29–44.

Philippot, P., Agrinier, P. & Scambelluri, M. (1998). Chlorine cycling in the subducted oceanic lithosphere. *Earth and Planetary Science Letters* **161**, 33–44.

Poli, S. & Schmidt, M. W. (2002). Petrology of subducted slabs. *Annual Review of Earth and Planetary Sciences* **30**, 207–335.

Putlitz, B., Valley, J. W., Matthews, A. & Katzir, Y. (2002). Oxygen isotope thermometry of quartz–Al_2SiO_5 veins in high-grade metamorphic rocks on Naxos island (Greece). *Contributions to Mineralogy and Petrology* **143**, 350–359.

Roedder, E. (1984). *Fluid Inclusions. Mineralogical Society of America, Reviews in Mineralogy* **12**, 644 pp.

Rumble, D., III & Yui T.-F. (1998). The Qinglongshan oxygen and hydrogen isotope anomaly near Donghai in Jiangsu Province, China. *Geochimica et Cosmochimica Acta* **62**, 3307–3321.

Rumble, D., III Giorgis, D., Ireland, T., Zhang, Z., Xu, H., Yui, T. F., Yang, J., Xu, Z. & Liou, J. G. (2002). Low $\delta^{18}O$ zircons, U–Pb dating, and the age of the Qinglongshan oxygen and hydrogen isotope anomaly near Donghai in Jiangsu Province, China. *Geochimica et Cosmochimica Acta* **66**, 2299–2306.

Ryabchikov, I. D. (1993). Fluid transport of ore metals in ultramafic mantle rocks. In: *Proceedings of the Eight Quadrennial IAGOD Symposium*. Stuttgart: Schweizerbart, pp. 425–433.

Scambelluri, M. & Philippot, P. (2001). Deep fluids in subduction zones. *Lithos* **55**, 213–227.

Scambelluri, M., Piccardo, G. B., Philippot, P., Robbiano, A. & Negretti, L. (1997). High salinity fluid inclusions formed from recycled seawater in deeply subducted alpine serpentinites. *Earth and Planetary Science Letters* **148**, 485–500.

Scambelluri, M., Bottazzi, P., Trommsdorff, V., Vannucci, R., Hermann, J., Gomez-Pugnaire, M. T. & Lòpez-Sànchez Vizcaìno, V. (2001). Incompatible element-rich fluids released by antigorite breakdown in deeply subducted mantle. *Earth and Planetary Science Letters* **192**, 457–470.

Schmidt, M. W., Vilzeuf, D. & Auzanneau, E. (2004). Melting and dissolution of subducting crust at high pressures: the key role of white mica. *Earth and Planetary Science Letters* **228**, 65–84.

Schreyer, W. (1999). Experimental aspects of UHP metamorphism: granitic systems. *International Geology Review* **41**, 701–710.

Selverstone, J., Franz, G., Thomas, S. & Getty, S. (1992). Fluid variability in 2 GPa eclogites as indicator of fluid behavior during subduction. *Contributions to Mineralogy and Petrology* **112**, 341–357.

Sharp, Z. D. (1990). A laser-based microanalytical method for the *in situ* determination of oxygen isotope ratios of silicates and oxides. *Geochimica et Cosmochimica Acta* **54**, 1353–1357.

Sharp, Z. D. (1995). Oxygen isotope geochemistry of the Al_2SiO_5 polymorphs. *American Journal of Science* **295**, 1058–1076.

Sharp, Z. D. & Barnes, J. D. (2004). Water soluble chlorides in massive seafloor serpentinites: a source of chloride in subduction zones. *Earth and Planetary Science Letters* **226**, 243–254.

Sharp, Z. D., Essene, E. J. & Smyth, J. R. (1992). Ultra-high temperatures from oxygen isotope thermometry of a coesite–sanidine grospydite. *Contributions to Mineralogy and Petrology* **112**, 358–370.

Smith, D. C. (1984). Coesite in clinopyroxene in the Caledonides and its implications for geodynamics. *Nature* **310**, 641–644.

Sobolev, N. V. & Shatsky, V. S. (1990). Diamond inclusions in garnets from metamorphic rocks: a new environment for diamond formation. *Nature* **343**, 742–746.

Sowerby, J. R. & Keppler, H. (2002). The effect of fluorine, boron and excess sodium on the critical curve in the albite–H_2O system. *Contributions to Mineralogy and Petrology* **143**, 32–37.

Stalder, R., Ulmer, P., Thompson, A. B. & Gunther, D. (2000). Experimental approach to constrain second critical end point in fluid/silicate systems: near-solidus fluids and melts in the system albite–H_2O. *American Mineralogist* **85**, 68–77.

Stalder, R., Ulmer, P., Thompson, A. B. & Günther, D. (2001). High pressure fluids in the system $MgO–SiO_2–H_2O$ at upper mantle conditions. *Contributions to Mineralogy and Petrology* **140**, 607–618.

Svensen, H., Jamtveit, B., Yardley, B., Engvik, A. K., Austrheim, H. & Broman, C. (1999). Lead and bromine enrichment in eclogite-facies fluids: extreme fractionation during lower-crustal hydration. *Geology* **27**, 467–470.

Thomas, R., Webster, J. D. & Heinrich, W. (2000). Melt inclusions in pegmatite quartz: complete miscibility between silicate melts and hydrous fluids at low pressure. *Contributions to Mineralogy and Petrology* **139**, 394–401.

Touret, J. L. R. (2001). Fluids in metamorphic rocks. *Lithos* **55**, 1–27.

Touret, J. L. R. & Frezzotti, M. L. (2003). Fluid inclusions in high pressure and ultrahigh pressure metamorphic rocks. In: Carswell, D. A. & Compagnoni, R. (eds) *Ultrahigh-pressure Metamorphism. European Mineralogical Union Notes in Mineralogy, 5*. Budapest: Eötvös University Press, pp. 467–487.

Tropper, P. & Manning, C. E. (2004). Paragonite stability at 700°C in the presence of $H_2O–NaCl$ fluids: constraints on H_2O activity and implications for high pressure metamorphism. *Contributions to Mineralogy and Petrology* **147**, 740–749.

Tropper, P. & Manning, C. E. (2005). The solubility of kyanite in $H_2O–SiO_2$ fluids at 800°C and 1 GPa: implications for Al–Si complexing in subduction-zone fluids. *EOS Transactions, American Geophysical Union* **86**(52), Fall Meeting Supplement, Abstract V31C-0621.

Ulmer, P. (1986). *NORM-Program for cation and oxygen mineral norms*. Zürich: Computer Library, Institute für Mineralogie und Petrographie, ETH-Zentrum.

Vannay, J. C., Sharp, Z. D. & Grasemann, B. (1999). Himalayan inverted metamorphism constrained by oxygen isotope thermometry. *Contributions to Mineralogy and Petrology* **137**, 90–101.

Vennemann, T. W. & O'Neil, J. R. (1993). A simple and inexpensive method of hydrogen isotope and water analysis of minerals and rocks based on zinc reagent. *Chemical Geology* **103**, 227–234.

Wallis, S., Enami, M. & Banno, S. (1999). The Sulu UHP Terrane—a review of the petrology and structural geology. *International Geology Review* **41**, 906–920.

Wunder, B., Rubie, D. C., Ross, C. R., Medenbach, O., Seifert, F. & Schreyer, W. (1993). Synthesis, stability, and properties of $Al_2SiO_4(OH)_2$: a fully hydrated analogue of topaz. *American Mineralogist* **78**, 285–297.

Wunder, B., Andrut, M. & Wirth, R. (1999). High-pressure synthesis and properties of OH-rich topaz. *European Journal of Mineralogy* **11**, 803–813.

Xia, Q.-K., Sheng, Y.-M., Yang, X.-Z. & Yu, H.-M. (2005). Heterogeneity of water in garnets from UHP eclogites, eastern Dabieshan, China. *Chemical Geology* **224**, 237–246.

Xiao, Y., Hoefs, J., van den Kerkhof, A. M., Fiebig, J. & Zheng, Y. (2000). Fluid history of UHP metamorphism in the Dabie Shan, China: a fluid inclusion and oxygen isotope study on the coesite-bearing eclogite from Bixiling. *Contributions to Mineralogy and Petrology* **139**, 1–16.

Xiao, Y., Hoefs, J. & van den Kerkhof, A. M. (2001). The Raobazhai complex in North Dabie Shan, China: eclogite- to granulite-facies metamorphism of subducted oceanic crust. *Journal of Metamorphic Geology* **19**, 3–19.

Xiao, Y. L., Hoefs, J., van den Kerkhof, A. M., Simon, K., Fiebig, J. & Zheng, Y. (2002). Fluid evolution during HP and UHP metamorphism in Dabie Shan, China: constraints from mineral chemistry, fluid inclusions and stable isotopes. *Journal of Petrology* **43**, 1505–1527.

Xiao, Y. L., Zhang, Z., Hoefs, J. & van den Kerkhof, A. M. (2006). Ultrahigh-pressure metamorphic rocks from the Chinese Continental Scientific Drilling Project: II oxygen isotope and fluid inclusion distributions through vertical sections. *Contributions to Mineralogy and Petrology* **152**, 443–458.

Yang, J. S., Wooden, J. L., Wu, C. L., Liu, F. L., Xu, Z. Q., Shi, R. D., Katayama, I., Liou, J. G. & Maruyama, S. (2003). SHRIMP U–Pb dating of coesite-bearing zircon from the ultrahigh-pressure metamorphic rocks, Sulu terrane, east China. *Journal of Metamorphic Geology* **21**, 551–560.

Ye, K., Yao, Y., Katayama, I., Cong, B., Wang, Q. & Maruyama, S. (2000). Large areal extent of ultrahigh-pressure metamorphism in the Sulu ultrahigh-pressure terrane of East China: new implications from coesite and omphacite inclusions in zircon of granitic gneiss. *Lithos* **52**, 157–164.

Young, E. D. (1993). On the $^{18}O/^{16}O$ record of reaction progress in open and closed metamorphic systems. *Earth and Planetary Science Letters* **117**, 147–167.

Yui, T.-F., Rumble, D. & Lo, C.-H. (1995). Unusually low $\delta^{18}O$ ultrahigh-pressure metamorphic rocks from the Sulu Terrain, eastern China. *Geochimica et Cosmochimica Acta* **59**, 2859–2864.

Zhai, M., Cong, J., Guo, J., Liu, Y. & Wang, Q. (2000). Sm–Nd geochronology and petrography of garnet pyroxene granulites in the northern Sulu region of China and their geotectonic implication. *Lithos* **52**, 23–33.

Zhang, R. Y., Hirajima, T., Banno, S., Cong, B. & Liou, J. G. (1995). Petrology of ultrahigh-pressure rocks from the southern Su-Lu region, eastern China. *Journal of Metamorphic Geology* **13**, 659–675.

Zhang, R. Y., Liou, J. G. & Ye, K. (1996). Petrography of UHPM rocks and their country rock gneisses. In: Cong, B. (ed.) *Ultrahigh-pressure Metamorphic Rocks in the Dabieshan–Sulu Region, China*. Beijing: Science Press, pp. 49–68.

Zhang, R. Y., Liou, J. G. & Shu, J. F. (2002). Hydroxyl-rich topaz in high-pressure and ultrahigh-pressure kyanite quartzites, with retrograde woodhouseite, from the Sulu terrane, eastern China. *American Mineralogist* **87**, 445–453.

Zhang, Z., Xu, Z. & Xu, H. (2000). Petrology of ultrahigh-pressure eclogites from the ZK703 drillhole in the Donghai, eastern China. *Lithos* **52**, 35–50.

Zhang, Z., Xiao, Y., Liu, F., Liou, J. G. & Hoefs, J. (2005a). Petrogenesis of UHP metamorphic rocks from Quinglongshan, southern Sulu, east–central China. *Lithos* **81**, 189–207.

Zhang, Z., Kun, S., Xiao, Y., van den Kerkhof, A. M. & Hoefs, J. (2005b). Fluid composition and evolution attending UHP metamorphism: study of fluid inclusions from drill cores, southern Sulu belt, eastern China. *International Geological Review* **47**, 297–309.

Zhang, Z., Shen, K., Xiao, Y., Hoefs, J. & Liou, J. G. (2006). Mineral and fluid inclusions in zircon of UHP metamorphic rocks from the CCSD-main drill hole: a record of metamorphism and fluid activity. *Lithos* **92**, 378–398.

Zheng, Y. F. (1993a). Calculation of oxygen isotope fractionation in anhydrous silicate minerals. *Geochimica et Cosmochimica Acta* **57**, 1079–1091.

Zheng, Y. F. (1993b). Calculation of oxygen isotope fractionation in hydroxyl-bearing silicates. *Earth and Planetary Science Letters* **120**, 247–263.

Zheng, Y. F., Fu, B., Gong, B. & Li, S. (1996). Extreme ^{18}O depletion in eclogite from the Su-Lu terrane in East China. *European Journal of Mineralogy* **8**, 317–323.

Zheng, Y. F., Fu, B., Li, Y., Xiao, Y. & Li, S. (1998). Oxygen and hydrogen isotope geochemistry of ultrahigh-pressure eclogites from the Dabie Mountains and the Sulu terrane. *Earth and Planetary Science Letters* **155**, 113–129.

Zheng, Y. F., Fu, B., Xiao, Y., Li, Y. & Gong, B. (1999). Hydrogen and oxygen isotope evidence for fluid–rock interactions in the stage of pre- and post-UHP metamorphism in the Dabie Mountains. *Lithos* **46**, 677–693.

Zheng, Y. F., Fu, B., Gong, B. & Li, S. (2003). Stable isotope geochemistry of ultrahigh pressure metamorphic rocks from the Dabie–Sulu orogen in China: implications for geodynamics and fluid regime. *Earth-Science Reviews* **1276**, 1–57.